NATIONAL ADVISORY COMMITTEE FOR AERONAUTICS

TECHNICAL NOTE 4155

AERODYNAMIC EFFECTS CAUSED BY ICING OF AN UNSWEPT NACA 65A004 AIRFOIL

By Vernon H. Gray and Uwe H. von Glahn

Lewis Flight Propulsion Laboratory
Cleveland, Ohio

Washington

February 1958

NATIONAL ADVISORY COMMITTEE FOR AERONAUTICS

TECHNICAL NOTE 4155

AERODYNAMIC EFFECTS CAUSED BY ICING OF AN UNSWEPT NACA 65A004 AIRFOIL

By Vernon H. Gray and Uwe H. von Glahn

SUMMARY

The effects of ice formations on the section lift, drag, and pitching-moment coefficients of an unswept NACA 65A004 airfoil section of 6-foot chord were studied. The magnitude of the aerodynamic penalties was primarily a function of the shape and size of the ice formation near the leading edge of the airfoil. The exact size and shape of the ice formations were determined photographically and found to be complex functions of the operating and icing conditions.

In general, icing of the airfoil at angles of attack less than 4° caused large increases in section drag coefficients (as much as 350 percent in 8 minutes of heavy glaze icing), reductions in section lift coefficients (up to 13 percent), and changes in the pitching-moment coefficient from diving toward climbing moments.

At angles of attack greater than 4° the aerodynamic characteristics depended mainly on the ice type. The section drag coefficients generally were reduced by the addition of rime ice (by as much as 45 percent in 8 minutes of icing). In glaze icing, however, the drag increased at these angles of attack. The section lift coefficients were variably affected by rime-ice formations; however, in glaze icing, lift increases at high angles of attack amounted to as much as 9 percent for an icing time of 8 minutes. Pitching-moment-coefficient changes in icing conditions were somewhat erratic and depended on the icing condition.

Rotation of the iced airfoil to angles of attack other than that at which icing occurred caused sufficiently large changes in the pitching-moment coefficient that, in flight, rapid corrections in trim might be required in order to avoid a hazardous situation.

INTRODUCTION

In evaluating the mission capability of an all-weather aircraft it is necessary to determine its performance in icing conditions. Information

concerning the aerodynamic penalties associated with icing of airframe components is therefore required. Research has been conducted by the NACA to determine the drag penalties associated with icing of several airfoils of thickness ratios from 9 to 12 percent (refs. 1 to 3). However, the only available data on lift and pitching-moment penalties due to icing of an airfoil are for an NACA 0011 airfoil section (ref. 3). These published aerodynamic data are useful for estimating the performance penalties in icing conditions for large transport and bomber aircraft, but are not readily applicable to high-speed high-altitude interceptor aircraft because such aircraft generally utilize a very thin airfoil (thickness ratio of the order of 4 percent). These interceptor aircraft cruise at altitudes at which little, if any, icing occurs. The icing problem of these aircraft is confined primarily to climb and descent, which are generally of short duration because of the high rates of climb and descent. The aircraft may occasionally be required to loiter during letdown at altitudes where icing can occur; however, because the over-all icing hazard is much reduced for these aircraft compared to conventional transport aircraft, the elimination of airframe icing protection equipment appears attractive. It is therefore necessary to determine the aerodynamic penalties caused by icing of thin airfoil sections in order to assess the need for icing protection equipment on lifting and control surfaces of high-speed interceptor aircraft.

In order to provide such data for use in interceptor-aircraft mission analyses, studies were made in the NACA Lewis icing tunnel of the aerodynamic penalties associated with icing of an unswept NACA 65A004 airfoil section of 6-foot chord. These studies included the effect of icing on the airfoil-section lift, drag, and pitching-moment coefficients. In addition, photographs of the cross sections of the ice formations causing the changes in the aerodynamic characteristics of the airfoil were obtained.

SYMBOLS

The following symbols are used herein:

α	corrected angle of attack, deg
C_D	corrected section drag coefficient
C_L	corrected section lift coefficient
C_M	corrected section pitching-moment coefficient about quarter-chord point
p_l	local static pressure on airfoil surface, lb/sq ft

p_0 free-stream static pressure, lb/sq ft

q_0 dynamic pressure, lb/sq ft

Subscript:

0 initial value before icing

Superscript:

' measured aerodynamic values (uncorrected)

APPARATUS

The model consisted of an NACA 65A004 airfoil section of 6-foot chord. (Coordinates for this section are given in ref. 4). The model was mounted vertically to span the 6-foot height of the Lewis icing tunnel (fig. 1). The airfoil was equipped with a 42-inch-span removable leading-edge section that provided for installation of a variety of icing protection systems. For this study, however, the removable section was constructed of wood and covered with a sheet of 0.010-inch-thick neoprene to prevent abrasion of the surface. The leading-edge section extended to 27 percent of the chord. The remainder of the airfoil section was constructed of stainless steel and was internally steam heated to prevent the accumulation of frost due to tunnel-air supersaturation and turbulence.

The airfoil was cantilevered from the tunnel balance frame by a mounting plate attached to the bottom of the airfoil. The balance frame was connected to a six-component force-balance system. Small air gaps were left between the mounting plate and the tunnel floor (approx. 1/4 in.) and between the airfoil and the tunnel ceiling (approx. 1/16 in.) to isolate the model from all but aerodynamic loads. Three forces on the airfoil (lift, drag, and pitching moment) were recorded simultaneously on tape by an electrically controlled printing mechanism at each balance scale.

The section drag of the model was also measured near the midspan with two side-by-side wake rakes, one mounted from the floor and one from the ceiling (fig. 1). These rakes were located about 38 inches behind the trailing edge of the airfoil. Each rake consisted of 80 electrically heated total-pressure tubes and five static-pressure tubes. The total-pressure tubes were spaced on 1/4-inch centers. The static-pressure tubes were evenly distributed on 5-inch centers along the span of the rakes either slightly above or below the total-pressure tubes.

The support struts for the rakes were air heated for icing prevention. Airfoil pressure distribution was measured at the midspan by means of plastic pressure belts. All pressure data were photographically recorded from multiple-tube manometers. For drag determination from the wake rakes, the manometer-board tubes were manifolded to provide an integrating-type manometer.

In order to obtain photographs of cross sections of the ice formations, the ice on the airfoil after an icing run was removed by a steam-heated ice scraper except for a narrow band in a chordwise plane normal to the surface. The camera was positioned near the airfoil leading edge and directed spanwise, nearly parallel to the leading edge. A black 1/4-inch-mesh wire grid was placed against the ice to provide a scale of measurement, and a white wire of the grid was alined to be an extension of the airfoil chord line. Further details of this technique are described in reference 5.

Liquid-water content was measured by means of a pressure-type icing-rate meter (ref. 6). Icing-cloud-droplet size as a function of spray-nozzle pressure settings was determined from a previous calibration of droplet size obtained with water droplets carrying dye in solution (ref. 7).

Following the conclusion of the lift, drag, and pitching-moment studies, the trailing-edge region of the airfoil section was removed at the 82-percent-chord station and modified to incorporate a simple hinged flap. This flap was also steam heated. The flap was remotely controlled and adjustable for flap angles of $\pm 15^{\circ}$ relative to the airfoil chord line. A strain-gage mechanism was installed to measure the flap hinge moment required to hold the flap at a specified angle. The hinge moment was recorded by a potentiometer.

CONDITIONS AND PROCEDURES

The nominal values for the range of icing conditions studied herein are:

Airspeed, knots	109 to 240
Reynolds number	$\sim 7 \times 10^6$ to 15.5×10^6
Geometric angle of attack, deg	0 to 12
Total air temperature, $^{\circ}F$	0, 10, and 25
Water content, g/cu m	0.45 to 2.0
Droplet diameter (volume median), microns	11 to 19
Flap angle, deg	-15 to +15

The specific combinations of water content, droplet size, and airspeed used in the icing tests are listed in table I. In general, the airfoil

was allowed to collect ice for periods of 3 to 17 minutes and data were recorded at about 1/2- to 2-minute intervals. Photographs were taken at the end of an icing period to record the shape and size of the ice formation.

In addition, ice formations were allowed to build up on the airfoil at a specified angle of attack for a particular icing time; the angle was then changed several times with the sprays turned off and aerodynamic data were recorded for the various positions. This procedure permitted an evaluation of the aerodynamic changes that might occur for (1) an aircraft letting down through an icing condition and then flaring out for a landing approach, or (2) an aircraft climbing through an icing condition and then cruising at altitude while retaining the ice formation accreted during climb.

In the evaluation of the effect of leading-edge ice formations on hinge moments, the following procedure was used: The airfoil was permitted to ice for a specified icing period; the flap was then moved over its range of $\pm 15^{\circ}$ and the moments were recorded; these data were then compared with similar measurements obtained in clear air with a clean leading edge.

The most convenient method of obtaining the desired aerodynamic data for the studies presented herein was by means of the balance system. However, a previous study (ref. 3) had shown that for certain operating conditions airfoil end effects caused by the air gaps between the model and the tunnel could result in appreciable errors in the determination of the airfoil aerodynamic characteristics. Consequently, the section lift and pitching-moment coefficients in clear air obtained from the balance system were checked against values obtained from an integration of the surface pressure distribution over the airfoil. Both normal and chordwise components of the pressure distribution were considered in these computations. The section drag coefficient in clear air obtained from the balance system was checked with values obtained from a momentum survey in the wake of the airfoil and also with values from an integration of the surface-pressure distribution.

A comparison of the lift and pitching-moment coefficients in clear air calculated from surface-pressure distributions with those measured with the balance system is shown in figure 2 for various geometric angles of attack α'. The agreement between the two methods indicates that the airfoil end effects were not significant with respect to lift and pitching moment. Therefore, the lift and pitching-moment values obtained with the balance system in icing conditions are believed to be valid.

A comparison of section drag coefficients in clear air obtained by three methods is shown in figure 3 for geometric angles of attack from 0° to 12°. For angles of attack greater than about 4°, generally good agreement is noted for the section drag calculated from the pressure

distribution and the balance system. However, at the higher angles of attack the drag calculated from the wake survey becomes progressively greater than that obtained by either of the other two methods. The equations developed for momentum losses in the wake (refs. 8 and 9) apparently do not apply at the higher angles of attack, probably because the airflow separates from the upper surface of the airfoil, as is discussed later in this report. For angles of attack from 0° to 4°, the section drag calculated from the wake survey is less than that obtained from the balance system, but from 0° to 2° is greater than that obtained from an integration of surface-pressure distribution. The high drag values measured with the balance system are attributed in part to the airfoil end effects (ref. 3). The section drag values obtained from an integration of the surface-pressure distributions are considered low because of problems inherent in the computations and because skin friction is not included in the pressure drag calculations. Accordingly, in the angle-of-attack range from 0° to 4°, the wake-survey values are considered to be the most valid.

Increases in section drag coefficients due to ice formations on the airfoil were substantially the same whether drag was measured with the balance system or by the wake-survey method (see also ref. 3). It was decided, therefore, that all initial values of lift, drag, and pitching-moment coefficients for the airfoil in clear air as well as changes in these coefficients due to icing would be based on measurements from the balance system, except for the initial drag values at geometric angles of attack of 4° and lower. These latter values would be obtained from wake-survey measurements.

All initial values of section lift, drag, and pitching-moment coefficients for the clean airfoil are corrected for tunnel-wall interference effects by use of equations given in reference 10. In general, compared with the measured values for the clean airfoil, the corrected lift was approximately 16 percent less, the corrected drag about 8 percent less, the corrected pitching moment up to 18 percent more negative at high angles of attack, and the corrected angle of attack a maximum of about 12 percent greater.

Analysis of the effect of tunnel-wall interference on changes in the airfoil aerodynamic characteristics caused by ice formations showed negligible corrections. To obtain absolute values of the respective coefficients for the iced airfoil, the corrected initial coefficients are added to the uncorrected changes in coefficients caused by icing.

Except as noted, the data shown are in terms of changes in the aerodynamic characteristics of the airfoil with duration in icing. In the calculations of all aerodynamic coefficients the increase in planform area caused by the ice formations (less than 3 percent) was neglected.

RESULTS AND DISCUSSION

Aerodynamic Characteristics of Airfoil in Clear Air

Aerodynamic coefficients. - The airfoil-section lift, drag, and pitching-moment coefficients corrected for tunnel-wall effects are shown as a function of angle of attack in clear air in figure 4. The slope of the lift curve is linear up to an angle of attack of about 4°. Near this angle a slight discontinuity in the lift curve is apparent, following which the slope of the lift curve is slightly reduced from that measured at the lower angles. The maximum lift coefficient, 0.93, occurred near an angle of attack of 11.5°. Beyond maximum lift there was not any sudden loss in lift. The lift characteristics of the airfoil at angles of attack greater than 4° are affected by flow separation occurring near the leading edge on the upper surface of the airfoil, as discussed in the appendix. The section drag coefficient increased slowly from about 0.006 at zero angle of attack to about 0.008 at 3°. For angles of attack greater than 3° the section drag coefficient increased rapidly and reached a value of about 0.22 at an angle of attack of 12.5° (see appendix). The section pitching-moment coefficient changed from zero to about -0.008 as the angle of attack was increased from zero to 3°. The pitching-moment coefficient then was nearly constant at a value of about -0.008 for angles of attack from 3° to 7°. At angles of attack greater than 7° the pitching moments progressively became more negative (to a value of -0.17 at an angle of attack of 12.5°), thus constituting larger diving moments (stable flight condition).

Pressure distribution. - The distribution of the pressure coefficient $\frac{p_l - p_0}{q_0}$ over the airfoil surface is tabulated in table II as a function of dimensionless surface distance from the zero-chord point for various geometric angles of attack up to 11°. Typical plots for several of these pressure distributions are shown in figure 5. The data shown in figure 5 indicate the presence of flow separation near the leading edge on the upper surface of the airfoil for geometric angles of attack greater than about 4°, as discussed in the appendix. This flow separation is associated with the large drag coefficients for these angles of attack (fig. 4).

The existence of this flow separation on the clean airfoil is of special interest in evaluating the aerodynamic characteristics of an iced airfoil. As discussed in the appendix, flow separation can be influenced by the size, shape, and location of ice on an airfoil. This effect of ice on flow separation helps to explain some of the changes in airfoil aerodynamic characteristics due to ice that are presented in the following sections.

Ice-Formation Characteristics

Typical photographs of ice formations observed on the leading-edge region of the airfoil are shown in figures 6 to 8. These ice formations fit into the general categories of glaze, intermediate, and rime ice. The glaze-ice formations (fig. 6(a)) are characterized by bluff nearly transparent ice caps that protrude from the surface normal to the local airstream.

The glaze ice is further characterized by the more positive ice angles. The ice angle is defined in reference 5 as the angle between the extended chord line and the ice edge first reached in going from the upper to the lower surface of the airfoil. The ice angle is considered positive if the ice edge is above the chord line and negative if the ice edge is below the extended chord line. Glaze-ice formations generally are produced by operating and icing conditions which result in relatively high impingement rates and low heat-transfer rates on the airfoil surface, which thereby permit the impinging droplets to run or flow along the surface before they freeze. Rime icing is characterized by a more streamlined opaque ice formation that protrudes forward into the airstream (fig. 6(b)). This type of ice formation is characterized by a small positive or a negative ice angle (usually negative at higher angles of attack). Rime-ice formations are generally produced by operating and icing conditions which result in low impingement and high heat-transfer rates, which cause the droplets to freeze at or near the point of impact. Ice formations that have some characteristics of both rime and glaze icing are herein arbitrarily categorized as intermediate ice (fig. 8(b)).

The change in shape of typical glaze- and rime-ice formations with icing time for an angle of attack of 2.2° is shown in figure 6. (All angles of attack mentioned hereinafter are corrected for tunnel-wall effects.) For the glaze-ice formation (fig. 6(a)) the primary ice accumulation occurs very near the leading edge of the airfoil. Aft of the primary ice cap a smaller broken ice formation is observed on the lower surface of the airfoil. The ice cap near the leading edge of the airfoil becomes larger with icing time and after 14 minutes in icing has assumed a pronounced double-peak formation with a positive ice angle of about 43°. The total projected frontal height of this ice formation is about $2\frac{3}{4}$ inches, or almost the same as the maximum airfoil thickness. The rime-ice formations in figure 6(b) show that the general shape of the ice cap does not change materially with icing time. The ice formation grows forward parallel to the local airstream and has a projected frontal height of about $1\frac{1}{2}$ inches after an icing time of 10 minutes.

Typical glaze-ice formations for angles of attack of 0° to 6.6° are shown in figure 7(a). These photographs show that for a glaze-ice formation at zero angle of attack a symmetrical double-peak ice formation is

formed near the leading edge of the airfoil and little or no ice is formed on the airfoil aft of the primary formation. The large ice cap shields the downstream surfaces of the airfoil from direct water-droplet impingement. At the 2.2° angle of attack the double-peak primary ice formation is also evident; however, it is unsymmetrical, and there is a broken ice formation on the lower surface. At the 4.4° angle of attack a true double-peak ice formation is not evident at the leading edge, and there is an increased quantity of ice on the lower surface. At an angle of attack of 6.6° an almost uniformly thick but broken ice formation extends aft on the lower surface for about 6 percent of chord before gradually tapering off in thickness as the limit of droplet impingement is approached. Impingement characteristics for the 65A004 airfoil are contained in references 4 and 5. The broken ice formations, which resemble ice clumps in the photographs, actually consisted of spanwise ice ridges. With increasing angle of attack less ice formed above the extended chord line on the upper surface of the airfoil.

4439

With rime icing (fig. 7(b)) the ice forms in the region of the greatest local impingement rate and faces into the airstream. At angles of attack greater than zero for this airfoil, rime ice forms an aerodynamic "nose flap". This nose flap, especially at high angles of attack, adds camber to the airfoil and thereby tends to improve some of the aerodynamic characteristics of the iced airfoil compared to the clean airfoil, as shown later.

CV-2

The effect of rate of water catch on the ice formation near the leading edge of the airfoil is shown in figure 8. With an increase in water-catch rate, the ice formation grows faster, becomes more characteristic of glaze icing, and projects into the airstream more normal than parallel to the local flow field. The alteration of ice shape with water content and drop size (both factors contributing to rate of water catch) is graphically illustrated in figure 8 by the change in the ice angle. As the water-catch rate increases, this angle becomes less negative and then positive.

Variation of Aerodynamic Characteristics with Icing Time, Ice Shape, and Angle of Attack

The changes in section lift, drag, and pitching-moment coefficients with icing time obtained in this study are shown in figures 9 and 10 for various constant angles of attack. Also shown in these figures are cross sections of the ice deposits on the leading-edge region of the airfoil. These sketches were traced from photographs of the ice taken at the end of the runs (similar to those shown in figs. 6 to 8) and depict the ice shapes for only about the forward 7 percent of the airfoil.

In general, analysis of the aerodynamic data and the ice-formation photographs showed that, in icing conditions, changes in the aerodynamic characteristics of the airfoil were related to the size and shape of the ice formations. The ice size and the resulting changes in aerodynamic coefficients generally increased progressively with increasing icing time. With ice classified as glaze, rime, or intermediate, the general trends in the aerodynamic changes due to ice shown in figures 9 and 10 can be summarized as follows:

Coefficient	Type of ice	Predominant type of change in coefficient at airfoil angle of attack of -						
		0°	2.2°	4.4°	6.6°	8.8°	10.6°	11.6°
Drag	Glaze	[a]+	+	+	+	+	nd	nd
	Intermediate	+	nd	+	0	-	-	~
	Rime	+	+	-	-	-	nd	-
Lift	Glaze	0	~	~	+	+	nd	nd
	Intermediate	0	nd	-	0	0	+	~
	Rime	0	-	~	0	-	nd	+
Pitching moment (b)	Glaze	0	+	+	~	-	nd	nd
	Intermediate	0	nd	+	+	0	-	+
	Rime	0	0	0	0	+	nd	+

[a]+ Increase ~ variable
- decrease nd no data
0 negligible

[b]Changes in pitching-moment coefficients are changes in direction rather than changes in magnitude; a change to a smaller negative value is a positive increment and is considered an increase.

The changes in aerodynamic coefficients caused by ice formations are functions of the ice type and angle of attack. For example, the drag coefficients always increased in glaze-icing conditions, whereas in rime-icing conditions drag decreased at angles of attack above about 4°. As expected, the intermediate ice type caused drag changes intermediate between those of rime and glaze icing. Consequently, zones of increasing and decreasing drag coefficients due to ice can be visualized in the foregoing table, and are separated by a dotted line as an aid in interpreting the trends. The trends of the lift and pitching-moment changes

due to ice are not as simple and consistent as are those of the drag coefficients. With some exceptions however, the lift coefficients generally increased because of icing at the higher angles of attack (above about 6° with glaze icing and above about 10° with intermediate and rime icing). At lower angles of attack lift generally decreased or changed negligibly because of icing. Pitching-moment changes due to ice were always positive increases or negligible, except between angles of attack of about 8° and 11° in glaze- or intermediate-icing conditions, where the values decreased.

The addition of ice to the airfoil was usually detrimental to its aerodynamic characteristics up to an angle of attack of about 4°. Above this angle, ice frequently improved the characteristics by reducing drag, increasing lift, and sometimes decreasing the pitching moment (increasing diving moment). Although these benefits did not generally all occur simultaneously, they did all occur at the 10.6° angle of attack with intermediate icing.

The preceding aerodynamic effects and trends with respect to ice formations on the 65A004 airfoil section cannot easily be explained with complete satisfaction; however, the following factors account for most of the observed effects. Below an angle of attack of about 4° good airflow over the clean airfoil exists, and the ice formations that build up in all types of icing conditions have the primary effects of adding roughness and flow spoilers to the surface, which add to the drag and reduce the lift. Above an angle of attack of about 4°, flow separates from the upper surface of the clean airfoil (see the appendix), resulting in large drag-coefficient increases and slight lift reductions. Rime-ice formations at these higher angles of attack form at negative ice angles and often resemble depressed nose flaps. Such "flaps" apparently assist airflow over the nose and reduce the extent of flow separation; consequently, the drag is reduced. Glaze-ice formations, even at these higher angles of attack, still constitute flow spoilers (with positive ice angles) and cause drag increases. However, the lift also generally increases with glaze ice on the airfoil, probably because of lift forces on the ice (which in this case acts as a raised nose flap), and possibly because the ice shape reduces the pressure bubble on the upper surface near the leading edge. It is also possible that lift decreases in rime-icing conditions are partially attributable to the ice formations that resemble depressed nose flaps. It is shown in reference 11 that a leading-edge flap on a symmetrical NACA 65A006 swept airfoil can reduce both lift and drag when depressed and can increase both lift and drag when raised. The complex trends in the lift and pitching-moment changes due to ice shown in figures 9 and 10 are the results of factors such as those described above, and the net effects depend on the relative magnitudes of the frequently opposing factors.

The magnitudes of aerodynamic changes due to ice, given both as absolute values and as percentage changes from the clean-airfoil coefficients, are shown in figure 11 as a function of angle of attack for three representative icing conditions for periods of 1 and 8 minutes. The curves show

that the absolute values of the aerodynamic coefficients generally change more at the higher angles of attack, but the percentage changes are generally greater at the lower angles of attack, because of the lower values of clean-airfoil coefficients (see fig. 4). In fact, for the examples shown, the greatest percentage increases in drag occurred at the 2.2° angle of attack. The largest percentage changes shown in figure 11 are as follows:

Coefficient	Greatest changes due to ice, percent of clean-airfoil coefficients	Angle of attack, deg	Type of ice
Lift	+8.7 -7.8	6.6 2.2	Glaze Glaze
Drag	+350 -45	2.2 6.6	Glaze Rime
Pitch	+65 -150	8.8 4.4	Glaze Intermediate

Herein, pitching-moment percentage changes are referenced to clean-airfoil values, which are negative; therefore, a change of +65 percent represents a change from a negative value to a more negative one (diving moment). It can be seen that sizable percentage changes may occur in the aerodynamic coefficients because of the addition of ice formations. Even larger changes may be found in the data of figures 9 and 10. For example, in figure 10(a) at an air temperature of 0° F a decrease of 0.028 in the lift coefficient due to ice represents a lift reduction below the clean-airfoil value of 13 percent. The large percentage changes in pitching moment can be considered negligible, however, because of the small values for the clean airfoil.

Effect of Icing Variables on Aerodynamic Characteristics

The previous section demonstrates the important effects of ice shape on the airfoil aerodynamic characteristics. Several icing variables affect the shape of an ice formation, for example, air temperature, liquid-water content, droplet size, icing time, airspeed, angle of attack, and airfoil impingement efficiencies. An analysis of the joint effects of these variables on the ice shape, based on the data presented herein, is given in reference 5. The analysis also includes an equation that correlates the general effect of these icing variables on the resultant aerodynamic drag changes due to the ice. In the paragraphs that follow, the effects of some of the icing variables on aerodynamic characteristics are illustrated merely by means of specific comparisons of data, wherein only one (or a minimum number) of the factors was varied.

Two examples of the effect of air temperature on the aerodynamic characteristics of the iced airfoil may be shown by comparing data from figures 10(a) and (f). These data, listed in the following table, were taken from the square symbols in both figures and were obtained at the following conditions: liquid-water content, 1.45 grams per cubic meter; airspeed, 152 knots; angles of attack, 2.2° and 8.8°; air temperatures, 0° and 25° F; and icing time, 8 minutes.

4439

Figure	Angle of attack, deg	Air temperature, °F	Change in aerodynamic coefficient due to icing		
			Drag	Lift	Pitching moment
10(a)	2.2	0	0.009	-0.028	0.008
10(a)	2.2	25	.017	0 to -.008	.008
10(f)	8.8	0	-.045	[a]0	.024
10(f)	[b]8.8	25	[c].012	[d].03	[e]-.02

[a]Maximum change during 8-minute icing period, -0.02.

[b]Ice shedding during run.

[c]Maximum change during 8-minute icing period, 0.019.

[d]Maximum change during 8-minute icing period, 0.064.

[e]Maximum change during 8-minute icing period, -0.032.

Increasing the air temperature from 0° to 25° F in both of these examples changed the ice type from rime to glaze and increased the drag and lift coefficients of the iced airfoil; the pitching-moment coefficients with ice on the airfoil at the 8.8° angle of attack became more negative, whereas at 2.2° no change occurred.

The initial rate of water catch, shown on figures 9 and 10, is a calculated term that includes the product of liquid-water content, airfoil impingement efficiency, and airspeed. This term is indirectly affected by droplet size and angle of attack, as these variables influence the airfoil impingement efficiency. An example of the effect of varying the initial rate of water catch on the aerodynamic characteristics of the iced airfoil, obtained from figure 10(c), is given in the following table. In this comparison, the following conditions were constant: airspeed, 152 knots; air temperature, 10° F; angle of attack, 4.4°; icing time, 6 minutes.

Initial rate of water catch, lb/(min)(ft span)	Type of ice	Change in aerodynamic coefficient due to ice		
		Drag	Lift	Pitching moment
0.045	Rime	-0.003	0	0.002
.092	Intermediate	.014	-.016	.014
.127	Glaze	.022	-.023	.002

Although these changes varied with icing time, the numbers quoted illustrate the general trends in this example; specifically, increasing the initial rate of water catch changed the ice from rime to glaze, increased the drag, decreased the lift, and variably affected the pitching-moment coefficients for the iced airfoil. Reference 5 shows that the initial rate of water catch remains nearly constant with icing time in a rime-icing condition, but in glaze-icing conditions the rate of water catch (determined by weight of ice collected) increased progressively with time in icing.

The effect of airspeed on the aerodynamic characteristics in icing is rather complex, and consequently, to quote specific examples might be misleading. Furthermore, the icing tests at angles of attack greater than 4.4° were conducted at only one airspeed. Therefore, the data of figures 9 and 10(a) to (d) should be referred to in estimating the airspeed effect for any specific condition of interest.

Aerodynamic Characteristics of Iced Airfoil Involving Changes in Angle of Attack

In flight, an aircraft may pass through an icing condition at one attitude (angle of attack) and then continue the flight in clear air at another attitude. Data were obtained to simulate this flight procedure and are presented in figure 12. The data are shown in this figure by the following: (1) a solid curve representing the clean-airfoil aerodynamic characteristics, (2) open symbols representing the aerodynamic data obtained when the airfoil was iced at a particular angle of attack and then rotated to other angles, and (3) solid symbols representing the aerodynamic coefficients obtained when the airfoil was iced at each of the various angles of attack shown by the symbols (same icing condition as for item (2)). These data are plotted as a function of angle of attack in figure 12. Data for item (3) were obtained from figure 10.

Rotation of an iced airfoil to higher angles of attack resulted in drag-coefficient increases significantly greater than those obtained when the airfoil was iced at the higher angles. For example, when the airfoil

was iced at the 2.2° angle of attack in glaze-icing conditions (open square symbols in fig. 12(b)) and rotated to 8.8°, a section drag coefficient of 0.137 was obtained, compared with a value of 0.100 when the airfoil was iced at 8.8° (solid square symbol). These values compare with the clean-airfoil drag coefficient of 0.112 at the 8.8° angle of attack. Rotation of an iced airfoil to lower angles of attack could result in either small drag reductions or increases compared to the values obtained when the airfoil was iced at the lower angles; however, the drag values in these cases were still much larger than the clean-airfoil values (figs. 12(d) and (e)).

Negative pitching-moment coefficients up to 12 times those obtained with a clean airfoil could be obtained by icing the airfoil at high angles of attack and then rotating the iced airfoil to lower angles. With ice formed at the 8.8° angle of attack, for example, the pitching-moment coefficient for the iced airfoil at angles between 2° and 7° (fig. 12(f)) averaged about -0.10 compared to the clean-airfoil value of about -0.008. Conversely, when the airfoil was iced at low angles of attack (0° and 2.2°) and then rotated to higher angles, the pitching moment compared to that for the clean airfoil generally became less negative, and frequently positive values of pitching moment were attained (figs. 12(a) and (b)).

Following an icing encounter, if a maneuver required a rapid sequence of angle-of-attack changes, considerable difficulty might be expected in attempting to adjust the aircraft trim to cope with the changes in magnitude and sense of the pitching moment.

Rotating an iced airfoil to other angles of attack resulted in lift coefficients comparable to those obtained when the airfoil was iced at these angles, and also comparable to those obtained for the clean airfoil. However, at angles of attack near 11° and 12°, with rime ice on the airfoil formed at low angles (figs. 12(a) and (b)), the lift coefficients of the iced airfoil were greater than those for the clean airfoil, probably because of the flap effect of the ice, as discussed previously.

Effect of Airfoil Ice Formations on Trailing-Edge Control-Surface Forces

Over a range of icing conditions considered to be glaze, and with angles of attack from 3.3° to 8.8°, flap angles up to ±15° and an airspeed of 152 knots, no significant effects on the control-surface hinge moments due to ice formations on the leading-edge region of the airfoil were obtained. The negligible change in control-surface hinge moment (and hence stick force) due to the icing is attributed to the inherently poor airflow over the upper surface of the airfoil. Apparently the ice formations on the leading-edge regions of the airfoil did not alter the airflow at the

control-surface station sufficiently to affect the control effectiveness. However, the control effectiveness for airfoils which normally have good upper-surface airflow might be more seriously affected by leading-edge ice formations than the thin airfoil studied herein.

SUMMARY OF RESULTS

A study of the effect of ice formations on the lift, drag, and pitching-moment characteristics of an unswept NACA 65A004 airfoil determined the following principal results:

1. The magnitude of the aerodynamic penalties was primarily a function of the shape and size of the ice formation near the leading edge of the airfoil. The size and shape of the ice formation in turn was a complex function of such variables as water content, droplet size, air temperature, icing time, airfoil angle of attack, and airspeed. (Empirical correlations among these variables, the ice shape, and aerodynamic drag due to ice are given in TN 4151, based on the present data.)

2. In general, icing of the airfoil at angles of attack less than 4° was detrimental to the aerodynamic characteristics. Icing caused large increases in section drag coefficient (as much as 350 percent in 8 minutes of heavy glaze icing), reductions in section lift coefficients (up to 13 percent), and changes in the pitching-moment coefficient from diving toward climbing moments.

3. At angles of attack greater than 4° the aerodynamic characteristics of the airfoil were at times either penalized or improved by ice formations on the airfoil, depending mainly on whether the ice was glaze or rime in character. In rime-icing conditions the section drag coefficient was generally reduced by icing compared to that for the clean airfoil (by as much as 45 percent in 8 minutes of icing). In glaze-icing conditions drag rises occurred at these higher angles of attack; however, the lift also increased, as much as 9 percent for an icing time of 8 minutes. Pitching-moment coefficients in icing conditions were somewhat erratic and depended on the icing condition.

4. Drag reductions due to ice on this airfoil were possible because at times the ice formations altered the aerodynamic shape sufficiently to reduce the extent of upper-surface flow separation below the amount present in clear air (beginning at an angle of attack near 4°). Lift increases due to ice were partly attributed to reductions in extent of flow separation and partly to lift forces on the ice itself, which at times was analogous to a leading-edge flap.

5. Rotation of the iced airfoil to angles of attack other than that at which icing occurred generally created aerodynamic effects different from those that resulted when the airfoil was iced at these angles; such rotation caused changes in the pitching-moment coefficient sufficiently large to indicate that difficulty might be expected in trim adjustment to avoid a hazardous flight situation in maneuvers requiring rapid changes in airfoil attitude with ice on the airfoil.

6. For the conditions investigated, no significant effects on trailing-edge control-surface hinge moments were determined as a result of ice formations on the leading-edge region of the airfoil.

Lewis Flight Propulsion Laboratory
National Advisory Committee for Aeronautics
Cleveland, Ohio, October 24, 1957

APPENDIX - EFFECT OF FLOW SEPARATION ON AERODYNAMIC CHARACTERISTICS OF AIRFOIL

The surface-pressure distribution over the airfoil is given in table II and is shown for several angles of attack in figure 5. These data show that a pressure bubble associated with flow separation occurs on the upper surface near the leading edge beginning at an angle of attack near 4° and extending to higher angles of attack. According to reference 12 the region of separated flow is characterized by boundary-layer flow separation near the leading edge followed by reattachment downstream on the airfoil surface. This flow separation is typical of thin low-drag airfoils at moderate and high angles of attack. The pressure bubble is characterized, as shown in figure 5, by a partially collapsed negative pressure peak followed by a region of approximately constant pressure (ref. 12). With increasing angle of attack the pressure peak is progressively reduced and the region of constant pressure is increased (fig. 5), which indicates greater regions of separated flow over the upper surface of the airfoil.

The flow separation over the upper surface of the airfoil resulted in a slight discontinuity of the lift curve near the 4° angle of attack (figs. 2 and 4). Beyond maximum lift there was no sudden redistribution of the surface pressures, hence, no abrupt loss in lift. The separation also resulted in an abrupt increase in drag near the 4° angle of attack. With increasing angle of attack the larger regions of separated flow also produced increasingly negative pitching moments.

On a thin airfoil, flow separation near the leading edge can be eliminated or its size and location altered by use of (1) increased airfoil leading-edge radius, (2) camber, (3) leading-edge flaps, and (4) flow disrupters, including protuberances, serrations, and roughness. Elimination or reduction of the pressure bubble will reduce the large drag rise observed at high angles of attack and may also result in improvements in the lift coefficient.

An ice formation may affect flow separation on a thin airfoil in any or all of the preceding ways. The effectiveness of the ice formation in delaying or eliminating flow separation is a function of the shape, size, and location of the ice. Consequently, the effect of ice on flow-separation characteristics depends on operating and icing conditions and the icing time.

REFERENCES

1. Gray, Vernon H., and von Glahn, Uwe H.: Effect of Ice and Frost Formations on Drag of NACA 65_1-212 Airfoil for Various Modes of Thermal Ice Protection. NACA TN 2962, 1953.

2. von Glahn, Uwe H., and Gray, Vernon H.: Effect of Ice Formations on Section Drag of Swept NACA 63A-009 Airfoil with Partial-Span Leading-Edge Slat for Various Modes of Thermal Ice Protection. NACA RM E53J30, 1954.

3. Bowden, Dean T.: Effect of Pneumatic De-Icers and Ice Formations on Aerodynamic Characteristics of an Airfoil. NACA TN 3564, 1956.

4. Brun, Rinaldo J., Gallagher, Helen M., and Vogt, Dorothea E.: Impingement of Water Droplets on NACA 65A004 Airfoil and Effect of Change in Airfoil Thickness from 12 to 4 Percent at 4° Angle of Attack. NACA TN 3047, 1953.

5. Gray, Vernon H.: Correlations Among Ice Measurements, Impingement Rates, Icing Conditions, and Drag Coefficients for an Unswept NACA 65A004 Airfoil. NACA TN 4151, 1957.

6. Perkins, Porter J., McCullough, Stuart, and Lewis, Ralph D.: A Simplified Instrument for Recording and Indicating Frequency and Intensity of Icing Conditions Encountered in Flight. NACA RM E51E16, 1951.

7. Gelder, Thomas F., Smyers, William H., Jr., and von Glahn, Uwe: Experimental Droplet Impingement on Several Two-Dimensional Airfoils with Thickness Ratios of 6 to 16 Percent. NACA TN 3839, 1956.

8. Goett, Harry J.: Experimental Investigation of the Momentum Method for Determining Profile Drag. NACA Rep. 660, 1939.

9. Block, Myron J., and Katzoff, S.: Tables and Charts for the Evaluation of Profile Drag from Wake Surveys at High Subsonic Speeds. NACA WR L-107, 1945. (Supersedes NACA RB L5F15a.)

10. Allen, H. Julian, and Vincenti, Walter G.: Wall Interference in a Two-Dimensional-Flow Wind Tunnel with Consideration of the Effect of Compressibility. Rep. 782, 1944. (Supersedes NACA WR A-63.)

11. Spreeman, Kenneth P.: Experimental Investigation at High Subsonic Speeds of the Effects of Leading-Edge Radius on the Aerodynamic Characteristics of a Sweptback-Wing - Fuselage Combination with Leading-Edge Flaps and Chord-Extensions. NACA RM L55E25a, 1955.

12. McCullough, George B., and Gault, Donald E.: Boundary-Layer and Stalling Characteristics of the NACA 64A006 Airfoil Section. NACA TN 1923, 1949.

TABLE I. - COMBINATIONS OF WATER CONTENT, DROPLET SIZE, AND AIRSPEED USED IN ICING STUDIES

Water content, g/cu m	0.45	0.63	0.90	0.95	1.20	1.40	1.45	1.86	2.00
Droplet diameter (volume median), microns	11.3	12.5	15.0	13.7	17.5	15.0	16.5	19.0	18.0
Airspeed, knots	240	240	240	152	240	109	152	152	109

TABLE II. - SURFACE-PRESSURE DISTRIBUTION

Surface location, ratio of surface distance to chord	Surface-pressure coefficient, $(p_l - p_0)/q_0$									
	Geometric angle of attack, α', deg									
(a)	0	1	2	3	4	5	6	8	10	11
-0.95	-0.014	-0.034	-0.038	-0.040	-0.051	-0.103	-0.097	-0.182	-0.447	-0.513
-.90	-.026	-.054	-.083	-.086	-.096	-.128	-.158	-.265	-.536	-.624
-.80	-.064	-.099	-.134	-.141	-.156	-.191	-.219	-.323	-.588	-.710
-.70	-.109	-.143	-.186	-.201	-.223	-.257	-.289	-.398	-.670	-.807
-.60	-.135	-.166	-.231	-.249	-.274	-.316	-.354	-.480	-.763	-.893
-.50	-.141	-.192	-.249	-.278	-.309	-.368	-.412	-.582	-.892	-1.02
-.40	-.170	-.224	-.297	-.332	-.376	-.434	-.482	-.738	-1.06	-1.16
-.35	-.148	-.211	-.287	-.332	-.382	-.451	-.514	-.850	-1.16	-1.23
-.30	-.148	-.211	-.291	-.342	-.405	-.477	-.563	-.997	-1.26	-1.29
-.25	-.116	-.192	-.279	-.339	-.414	-.507	-.637	-1.17	-1.36	-1.34
-.20	-.116	-.211	-.298	-.367	-.459	-.569	-.772	-1.38	-1.45	-1.38
-.16	-.116	-.214	-.328	-.409	-.506	-.655	-.965	-1.53	-1.53	-1.40
-.12	-.109	-.227	-.357	-.457	-.573	-.796	-1.27	-1.66	-1.60	-1.41
-.10	-.100	-.227	-.371	-.486	-.621	-.905	-1.43	-1.68	-1.62	-1.42
-.08	-.084	-.227	-.390	-.524	-.694	-1.09	-1.62	-1.69	-1.64	-1.43
-.06	-.087	-.240	-.433	-.591	-.825	-1.36	-1.75	-1.67	-1.62	-1.41
-.05	-.084	-.259	-.468	-.649	-.933	-1.54	-1.79	-1.66	-1.62	-1.40
-.04	-.103	-.291	-.539	-.744	-1.08	-1.72	-1.80	-1.64	-1.61	-1.39
-.03	-.103	-.329	-.613	-.866	-1.27	-1.89	-1.82	-1.65	-1.61	-1.39
-.02	-.122	-.425	-.774	-1.11	-1.61	-1.94	-1.84	-1.70	-1.66	-1.45
-.015	-.135	-.508	-.928	-1.35	-1.88	-2.02	-2.10	-1.99	-1.81	-1.48
-.010	-.154	-.617	------	-1.70	-2.29	-2.63	-2.91	-2.77	-2.28	-2.17
-.0075	-.138	-.693	-1.37	-2.05	-2.71	-3.20	-3.22	-3.21	-2.73	-2.81
-.0050	-.016	-.700	-1.47	-2.34	-3.10	-3.47	-3.26	-3.35	-2.97	-3.06
-.0025	.145	-.882	-2.43	-3.93	-5.21	-5.51	-4.17	-4.00	-3.23	-3.36
0	.984	.655	-.276	-2.04	-3.67	-4.54	-4.09	-4.51	-3.81	-4.09
.0025	.151	.738	.980	.955	.752	.546	.463	.191	.082	.016
.0050	-.177	.374	.747	.955	.994	.987	.958	.881	.835	.801
.010	-.215	.188	.498	.738	.860	.928	.965	.997	1.00	.995
.015	-.170	.150	.411	.623	.745	.832	.881	.942	.969	.957
.02	-.154	.118	.347	.540	.659	.750	.804	.878	.907	.903
.03	-.151	.073	.262	.431	.541	.632	.688	.772	.809	.812
.04	-.138	.054	.219	.374	.475	.559	.617	.701	.742	.742
.06	-.132	.022	.155	.291	.379	.454	.514	.599	.639	.640
.08	-.135	0	.115	.240	.319	.388	.444	.520	.562	.565
.10	-.135	-.006	.094	.201	.274	.342	.389	.466	.495	.500
.15	-.151	-.051	.031	.125	.191	.247	.289	.357	.381	.392
.20	-.161	-.070	-.007	.080	.134	.184	.225	.286	.299	.307
.25	-.170	-.089	-.031	.048	.096	.138	.174	.228	.232	.231
.35	-.158	-.096	-.052	.016	.054	.089	.116	.153	.150	.145
.45	-.135	-.089	-.053	.003	.032	.063	.084	.105	.082	.081
.55	-.135	-.096	-.070	-.022	.006	.026	.039	.048	.010	.005
.65	-.116	-.089	-.070	-.026	-.006	.007	.013	.010	-.046	-.059
.75	-.103	-.083	-.073	-.035	-.022	.020	-.013	-.037	-.113	-.134
.85	-.051	-.042	-.034	-.010	-.003	-.007	-.013	-.051	-.155	-.188
.95	-.014	-.020	-.014	0	-.088	0	-.006	-.006	-.210	-.266

[a]Negative sign in this column denotes upper-surface location (measured from zero-chord point), positive sign, lower-surface location.

Figure 1. - NACA 65A004 airfoil section installed in 6- by 9-foot test section of icing tunnel.

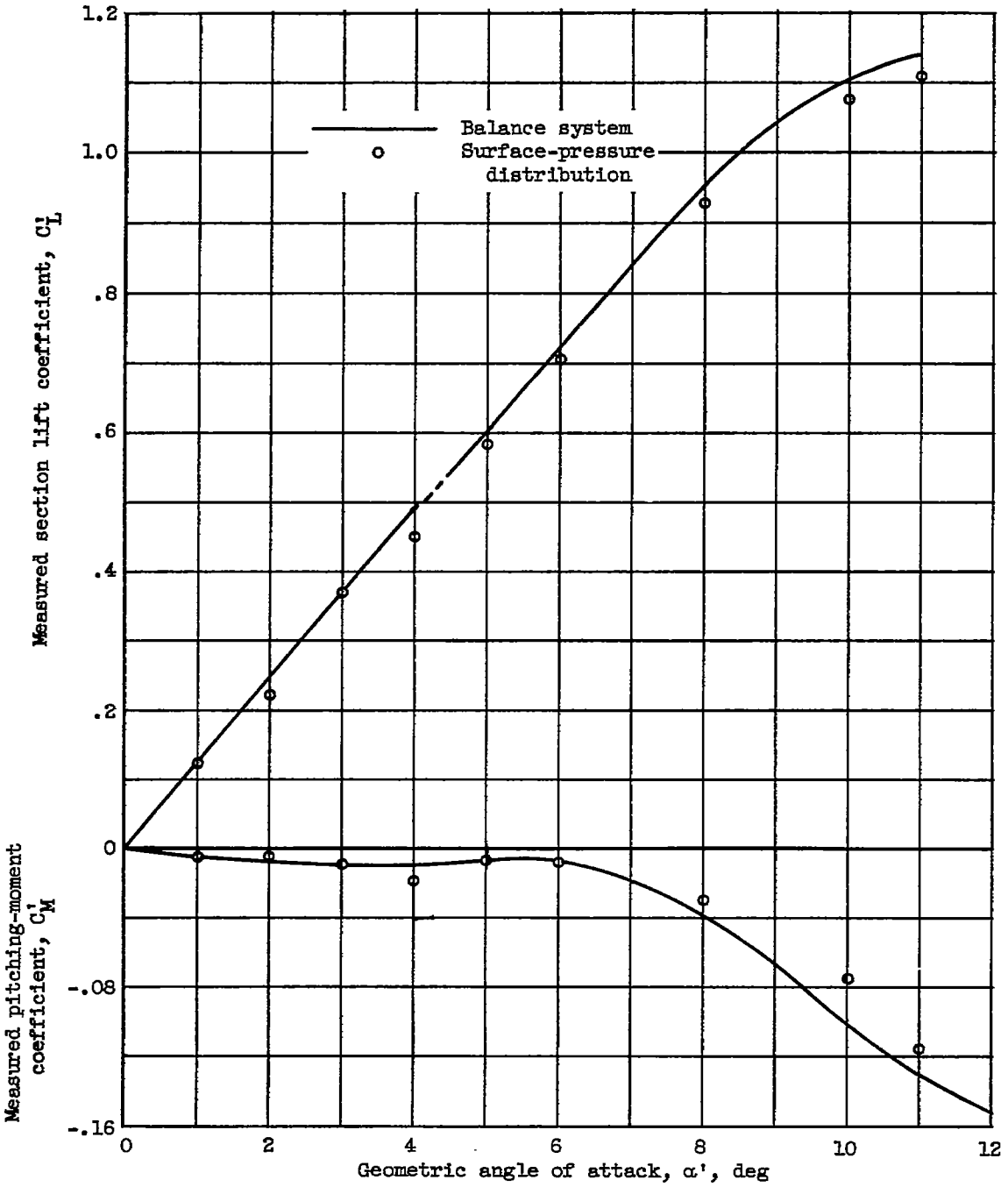

Figure 2. - Comparison of experimental section lift and pitching-moment coefficients determined from measurements using surface-pressure distributions and balance system.

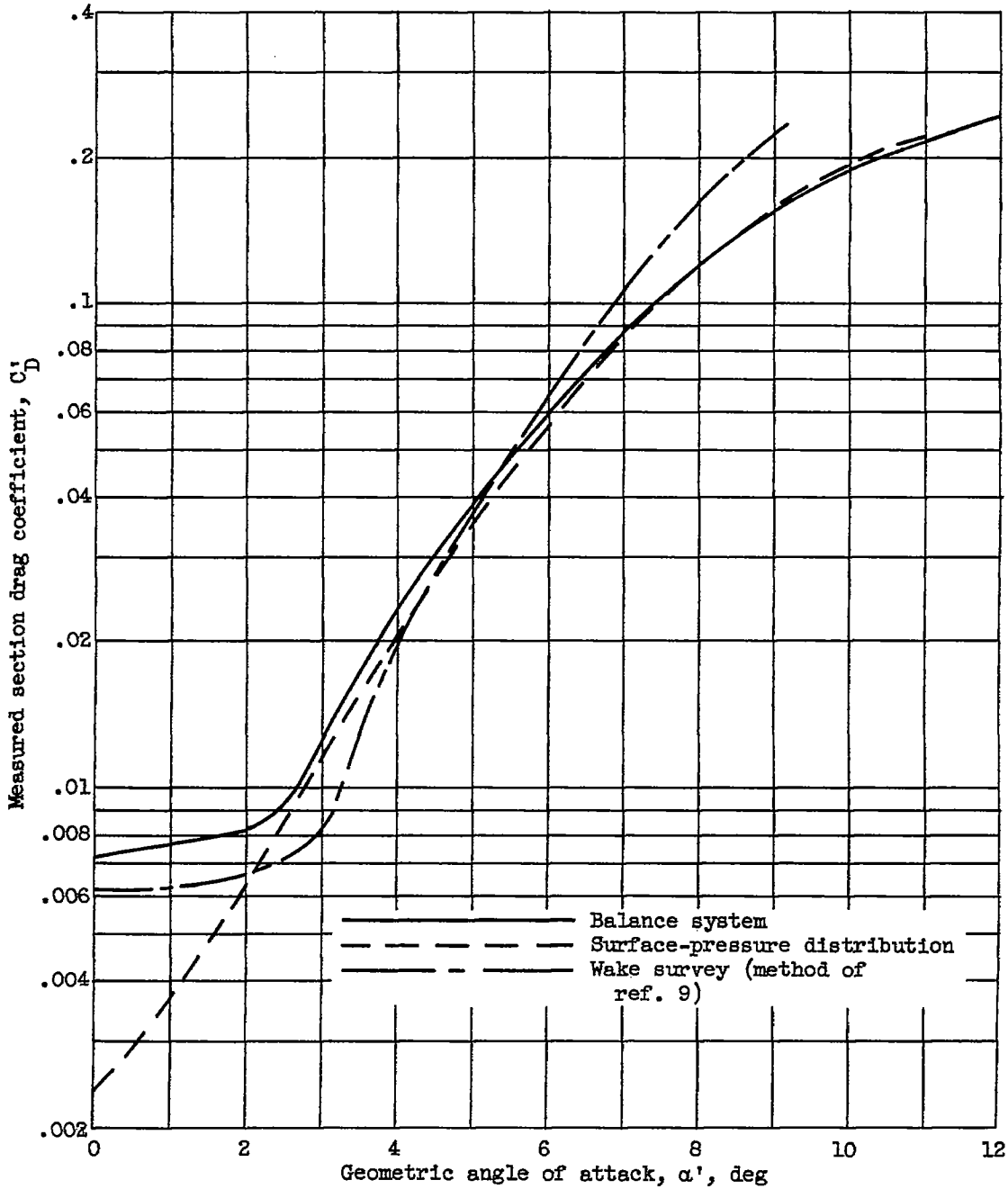

Figure 3. - Comparison of average values of section drag coefficient obtained by three methods of measurement.

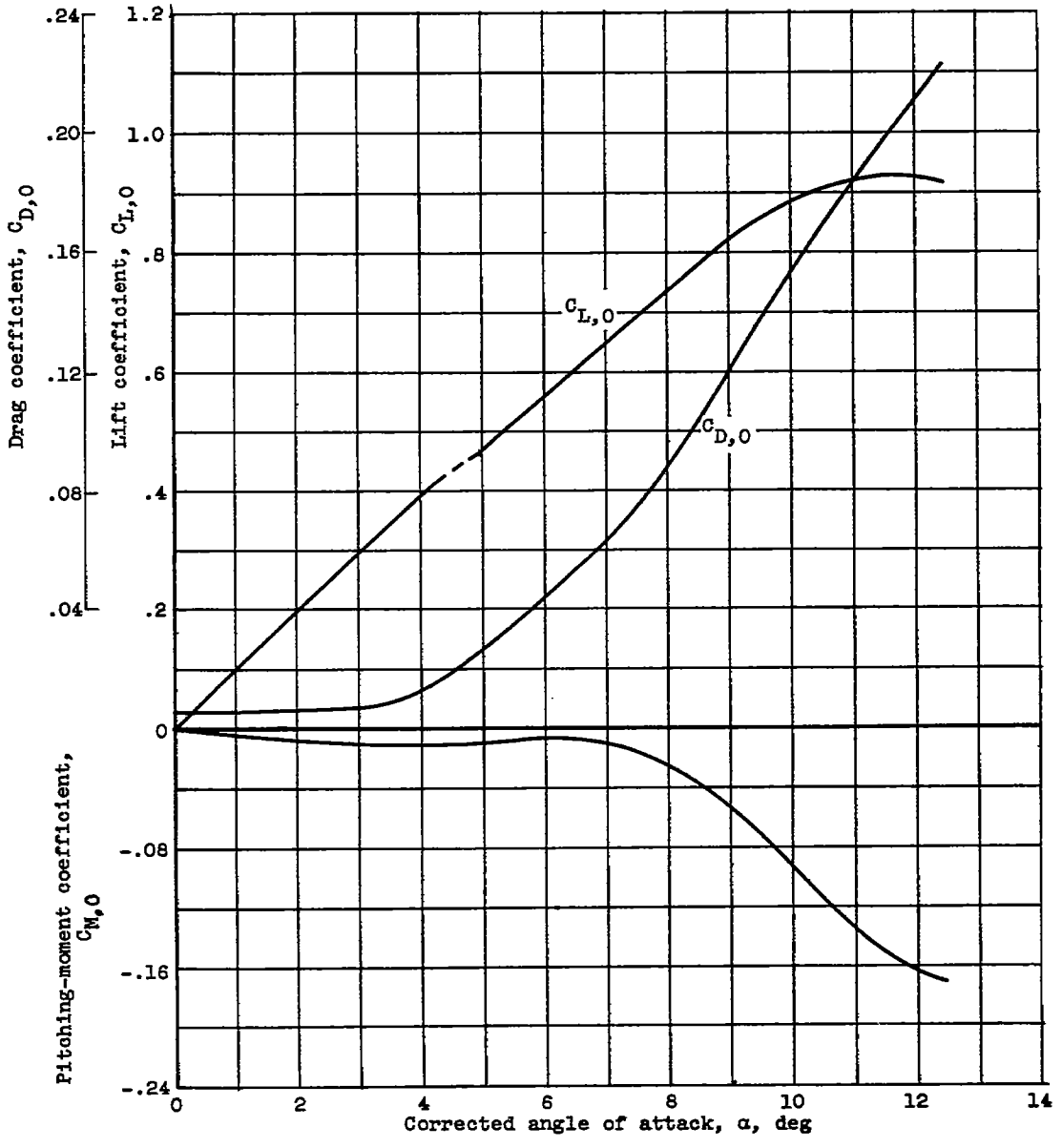

Figure 4. - Aerodynamic section characteristics of clean airfoil corrected for tunnel-wall effects.

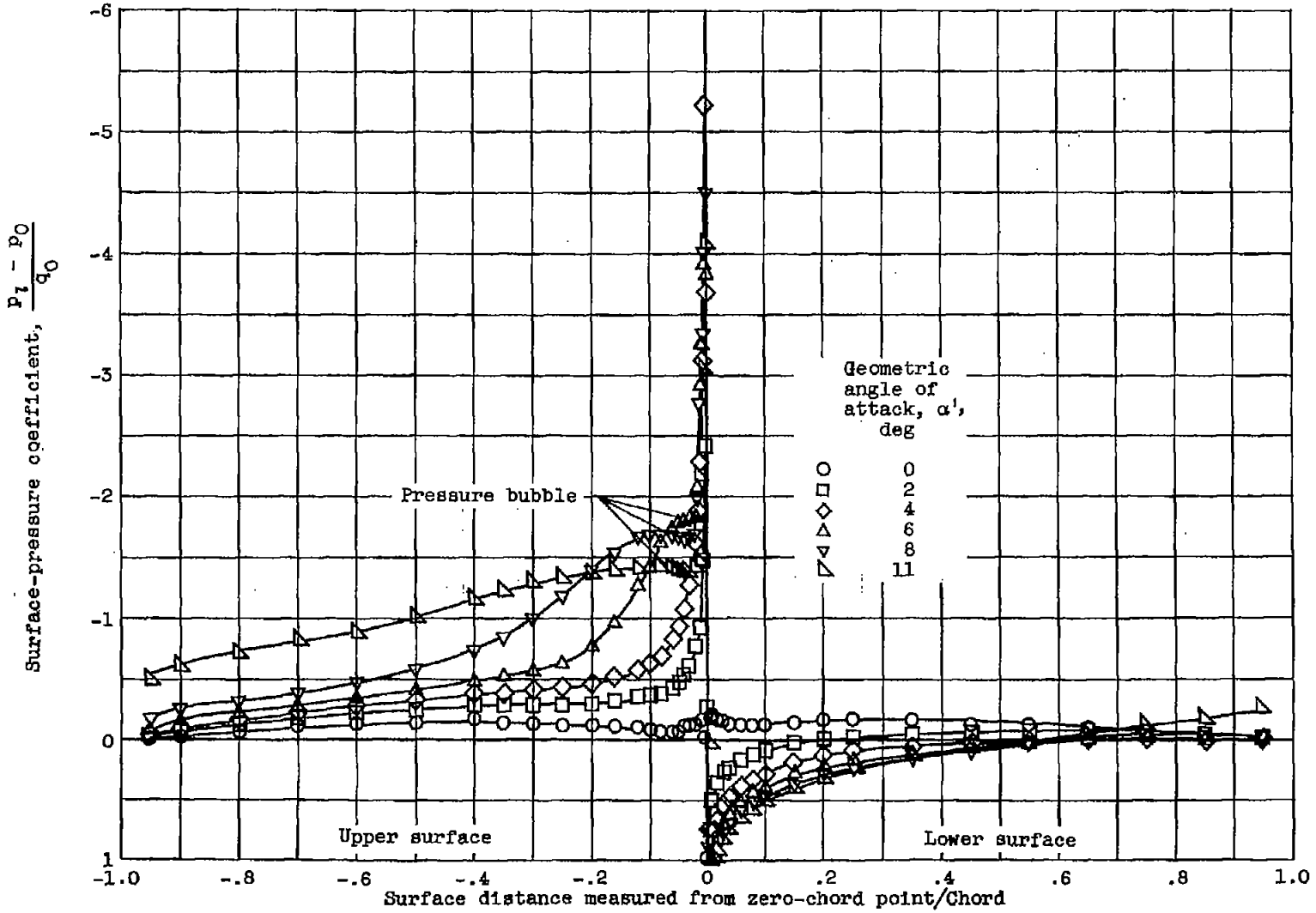

Figure 5. - Local-pressure distribution over airfoil.

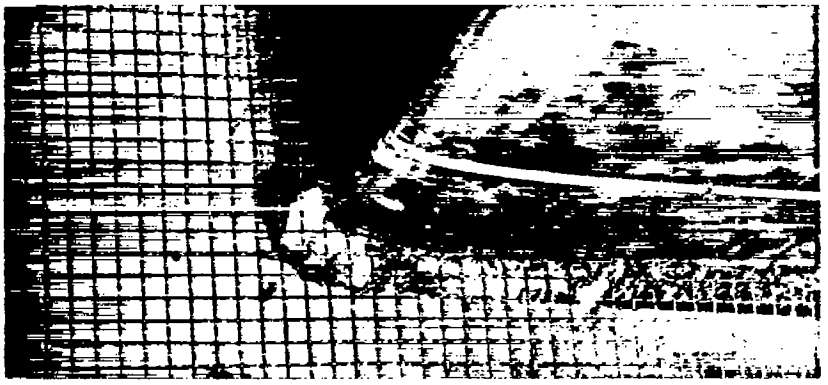

Icing time, 3 min

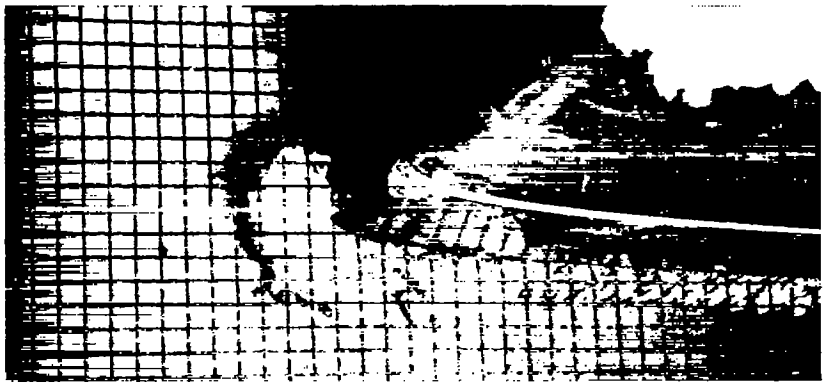

Icing time, 7 min

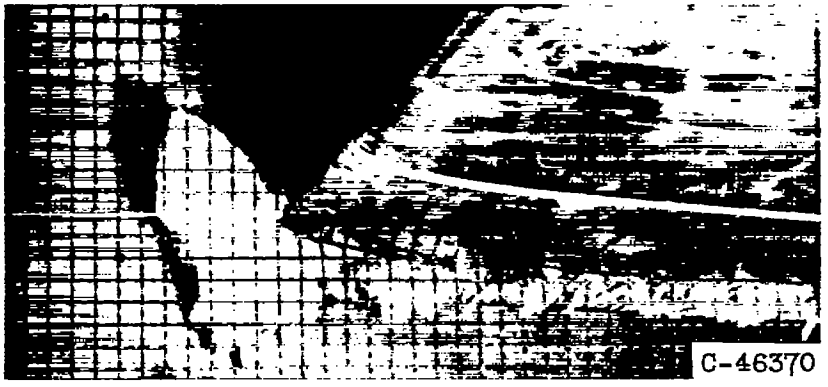

Icing time, 14 min

(a) Glaze ice; air temperature, 25° F.

Figure 6. - Typical variation of ice shape with time in icing. Angle of attack, 2.2°; airspeed, 152 knots; water content, 1.45 grams per cubic meter; droplet size, 16.5 microns.

Icing time, 5 min

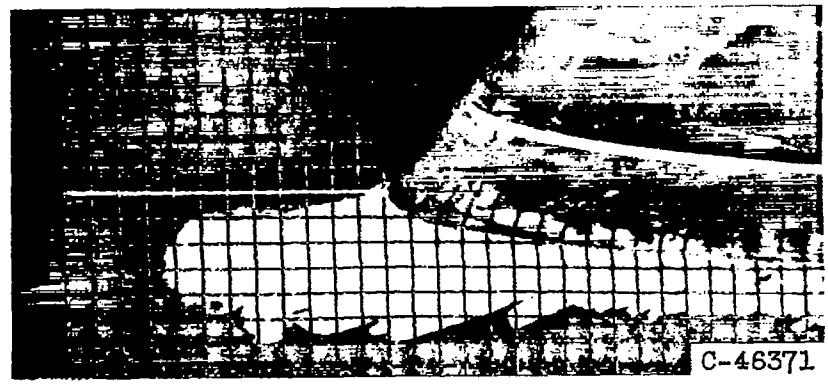

Icing time, 10 min

(b) Rime ice; air temperature, 0° F.

Figure 6. - Concluded. Typical variation of ice shape with time in icing. Angle of attack, 2.2°; airspeed, 152 knots; water content, 1.45 grams per cubic meter; droplet size, 16.5 microns.

Angle of attack, 0°; icing time, 12 min

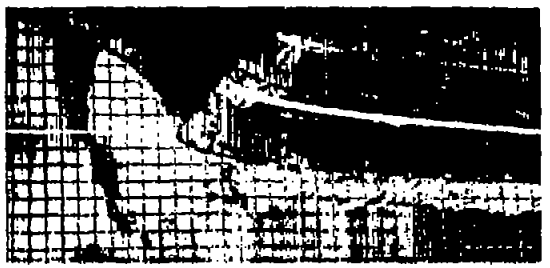

Angle of attack, 2.2°; icing time, 14 min

Angle of attack, 4.4°; icing time, 12 min

Angle of attack, 6.6°; icing time, 10 min

(a) Glaze ice; air temperature, 25° F; water content, 1.45 grams per cubic meter; droplet size, 16.5 microns.

Figure 7. - Typical variation of ice shape with angle of attack. Airspeed, 152 knots.

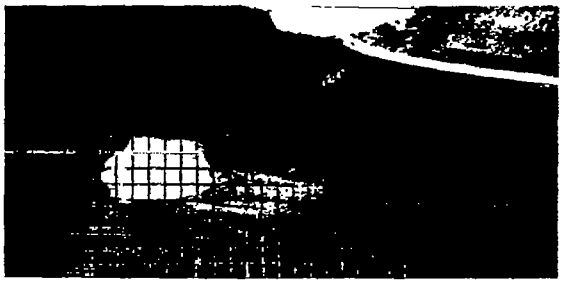

Angle of attack, 0°; icing time, 10 min

Angle of attack, 2.2°; icing time, 12 min

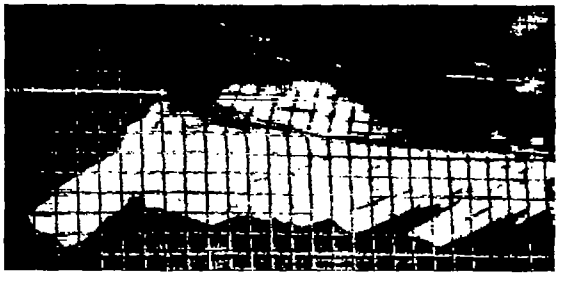

Angle of attack, 6.6°; icing time, 13 min

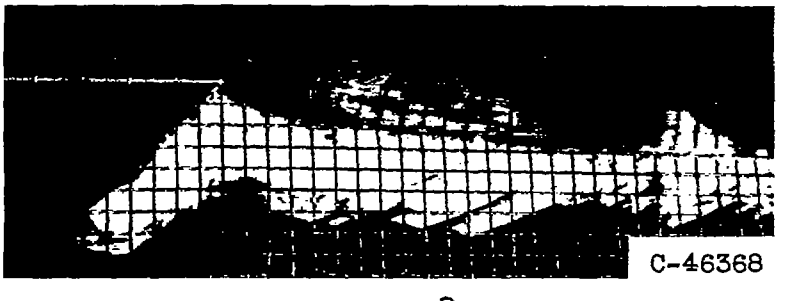

Angle of attack, 8.8°; icing time, 12 min

(b) Rime ice; air temperature, 10° F; water content, 0.95 gram per cubic meter; droplet size, 13.7 microns.

Figure 7. - Concluded. Typical variation of ice shape with angle of attack. Airspeed, 152 knots.

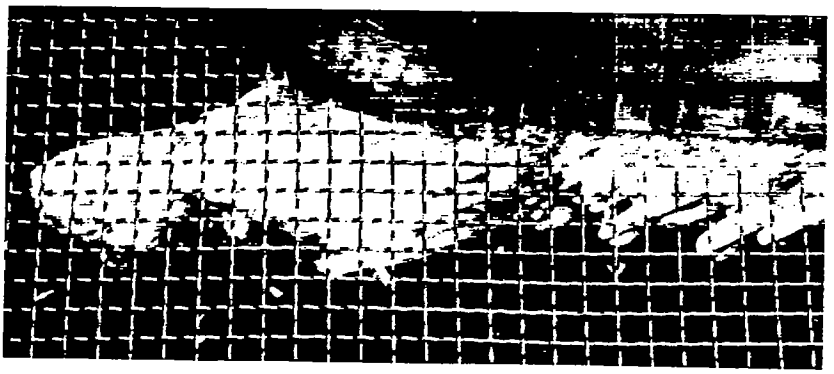

(a) Initial rate of water catch, 0.045 pound per minute per foot span; water content, 0.95 gram per cubic meter; droplet size, 13.7 microns; icing time, 13 minutes; rime ice formation.

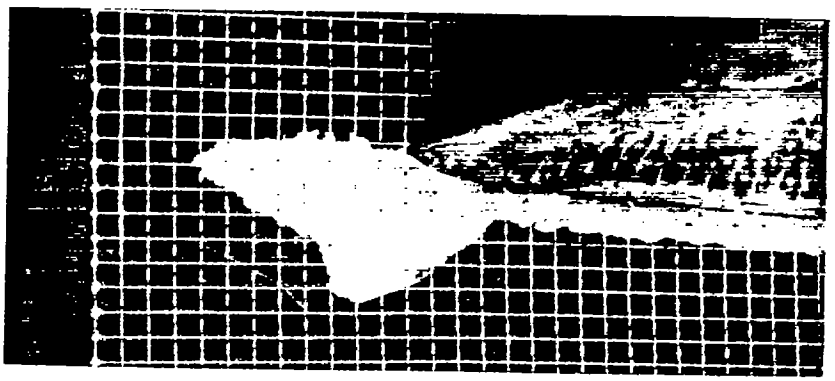

(b) Initial rate of water catch, 0.092 pound per minute per foot span; water content, 1.45 grams per cubic meter; droplet size, 16.5 microns; icing time, 10 minutes; intermediate ice formation.

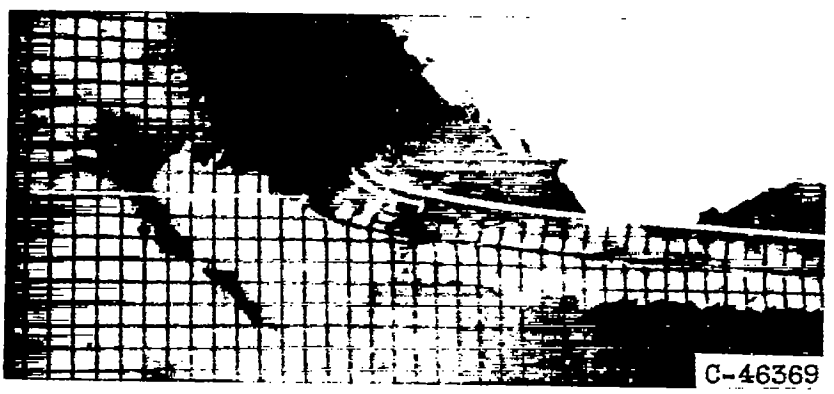

(c) Initial rate of water catch, 0.127 pound per minute per foot span; water content, 1.86 grams per cubic meter; droplet size, 19.0 microns; icing time, 9 minutes; glaze ice formation.

Figure 8. - Typical variation of ice shape with rate of water catch. Angle of attack, 4.4°; airspeed, 152 knots; air temperature 10° F.

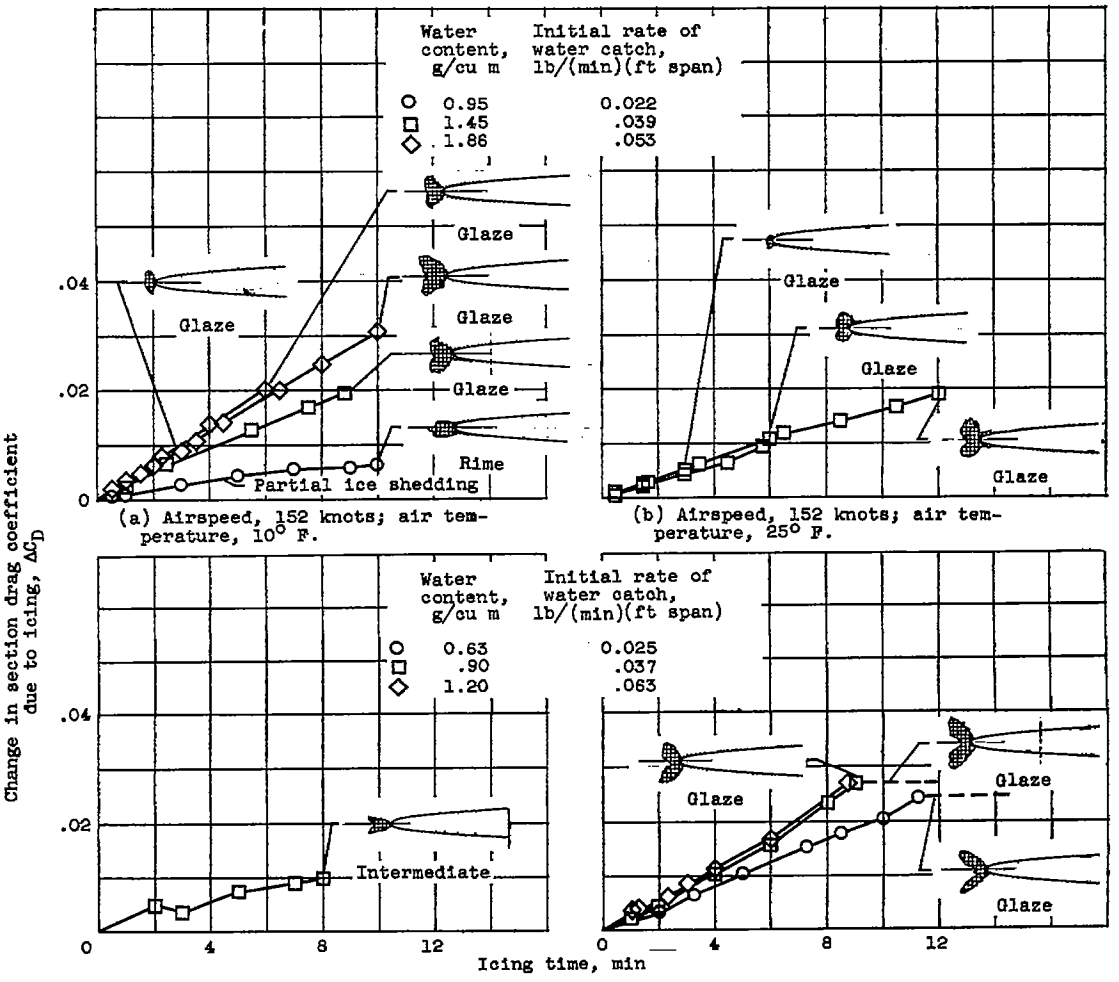

(a) Airspeed, 152 knots; air temperature, 10° F.

(b) Airspeed, 152 knots; air temperature, 25° F.

(c) Airspeed, 240 knots; air temperature, 10° F.

(d) Airspeed, 240 knots; air temperature, 25° F.

Figure 9. - Variation of section drag coefficient with icing time. Angle of attack, 0°.

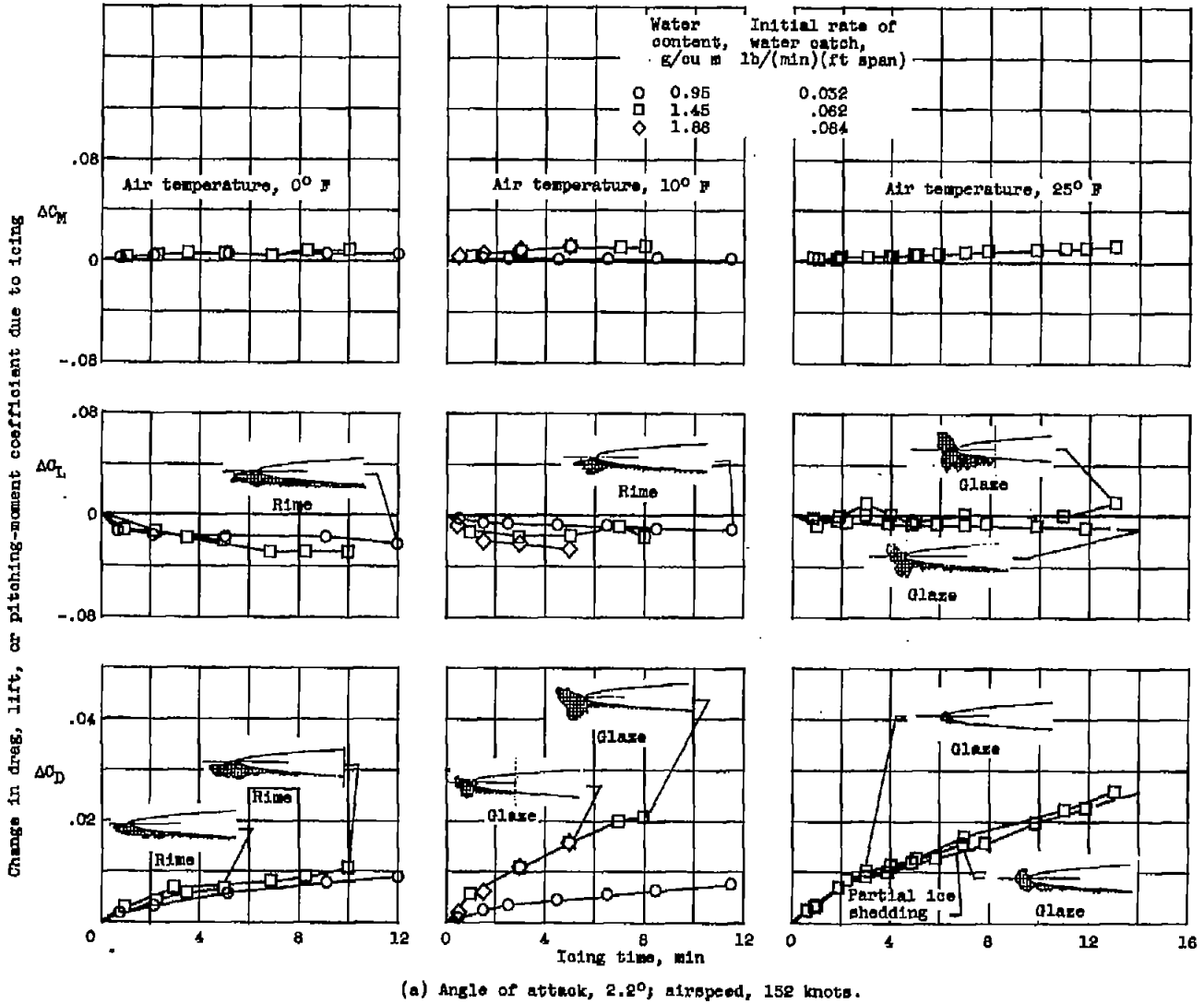

(a) Angle of attack, 2.2°; airspeed, 152 knots.

Figure 10. - Variation of aerodynamic coefficients with icing time.

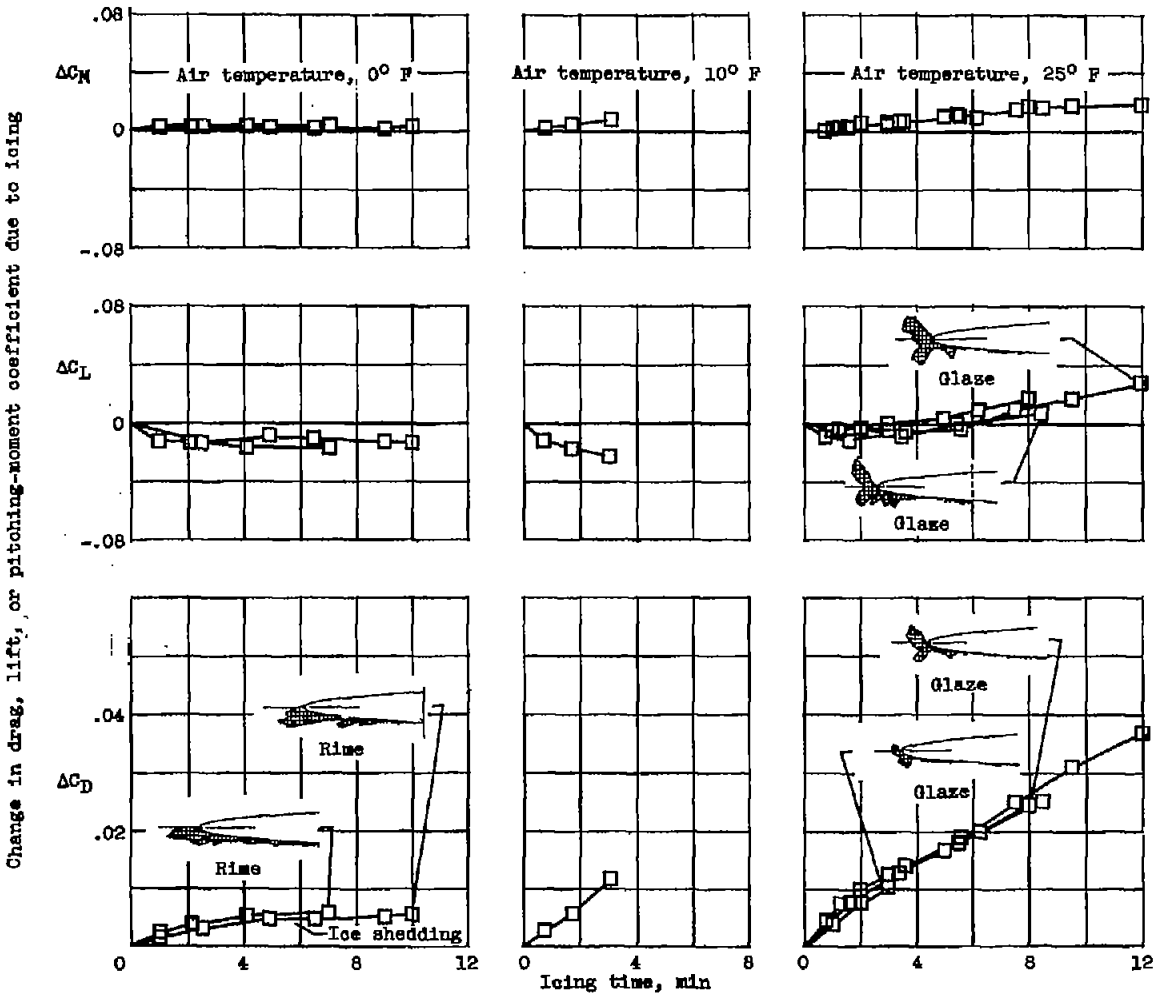

(b) Angle of attack, 2.2°; airspeed, 240 knots; water content, 0.90 gram per cubic meter; initial rate of water catch, 0.087 pound per minute per foot span.

Figure 10. - Continued. Variation of aerodynamic coefficients with icing time.

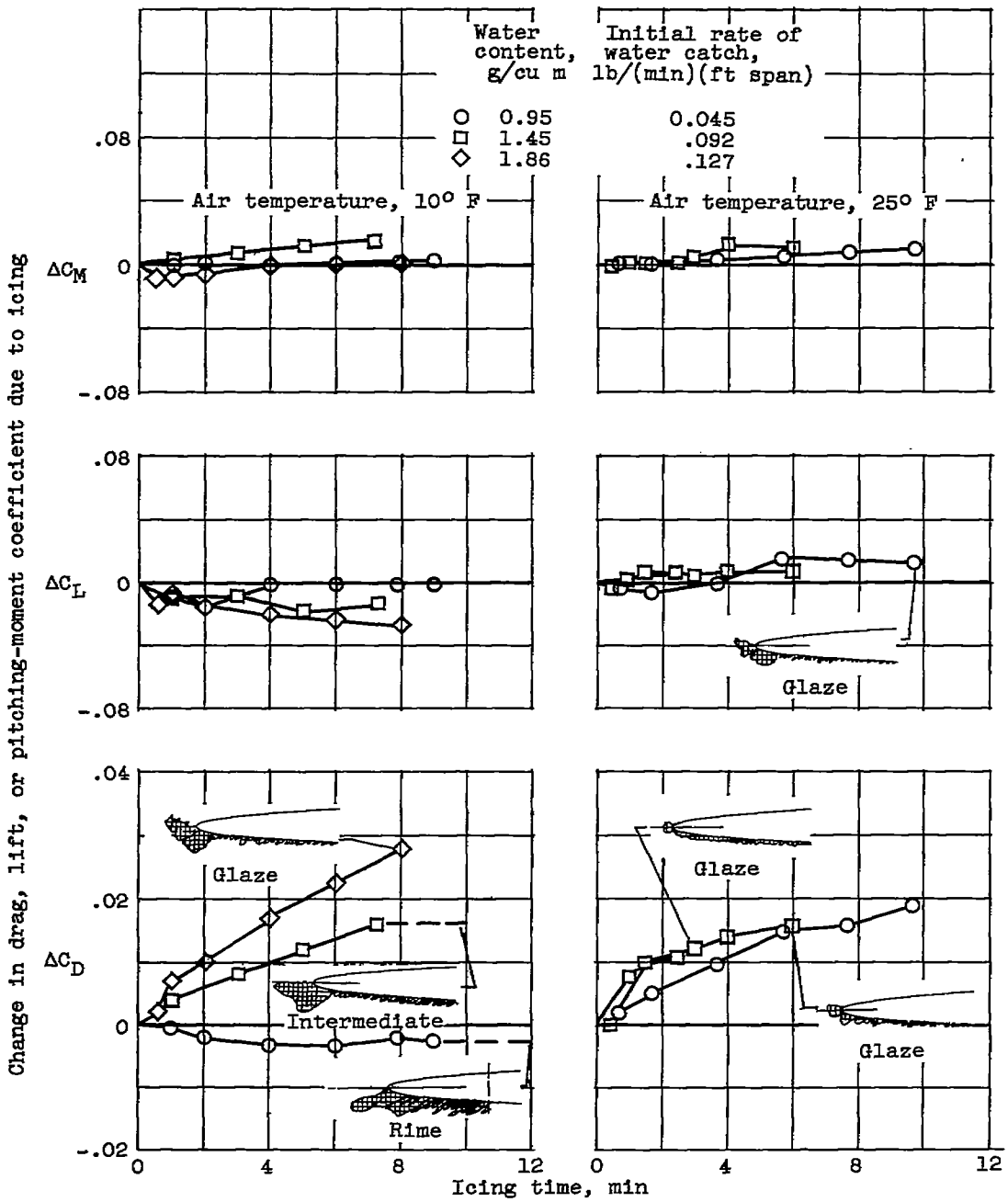

(c) Angle of attack, 4.4°; airspeed, 152 knots.

Figure 10. - Continued. Variation of aerodynamic coefficients with icing time.

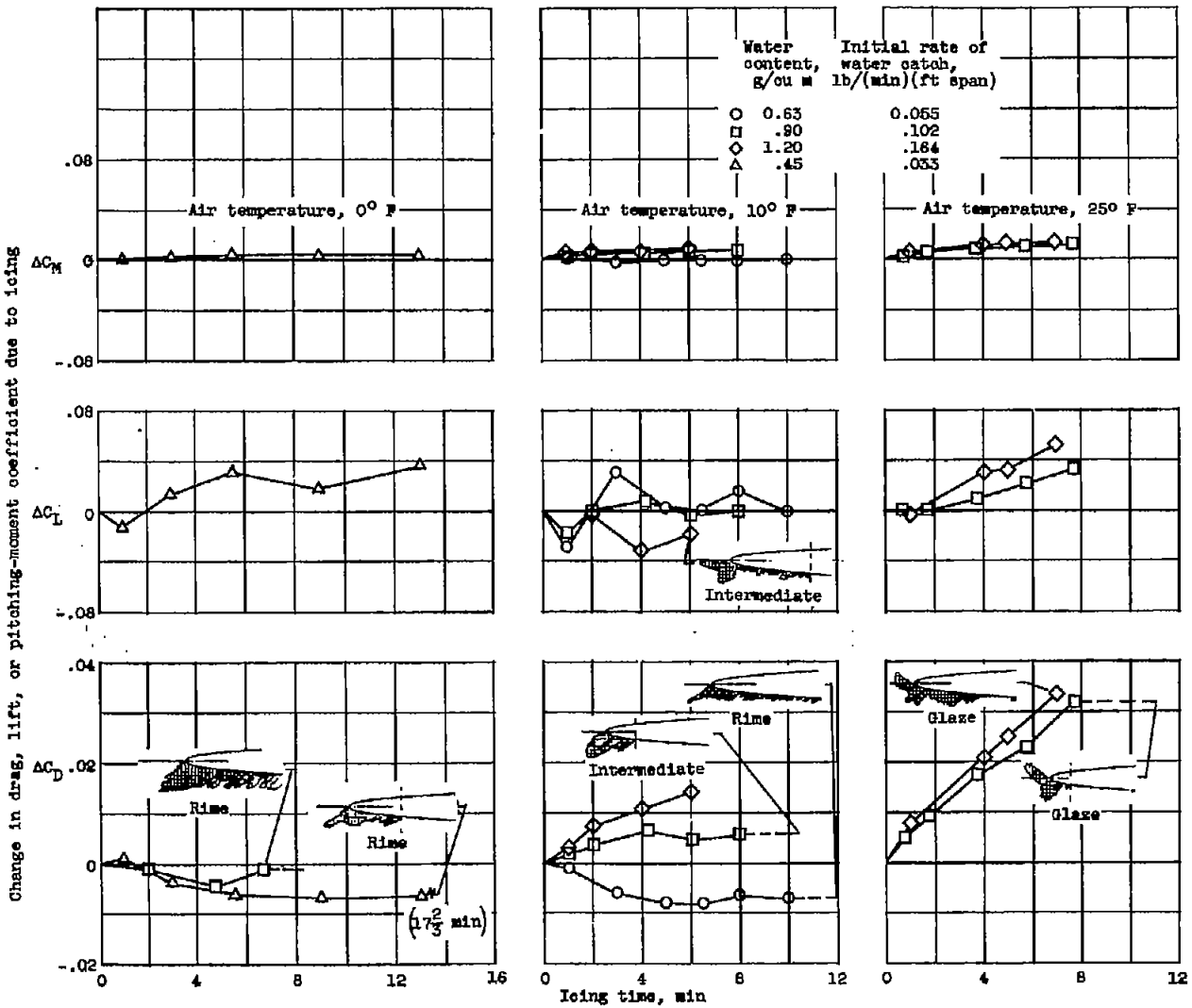

(d) Angle of attack, 4.4°; airspeed, 240 knots.

Figure 10. - Continued. Variation of aerodynamic coefficients with icing time.

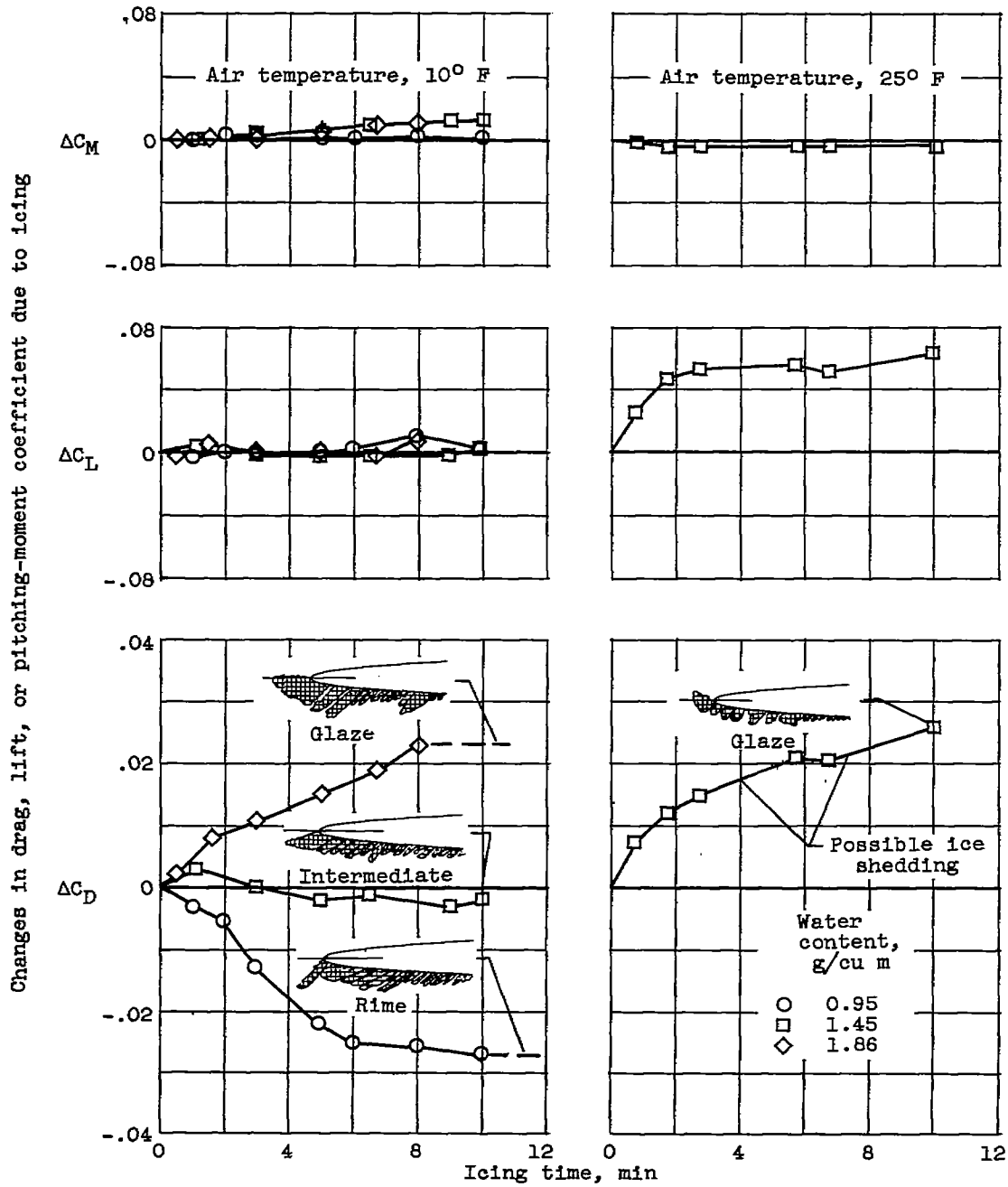

(e) Angle of attack, 6.6°; airspeed, 152 knots.

Figure 10. - Continued. Variation of aerodynamic coefficients with icing time.

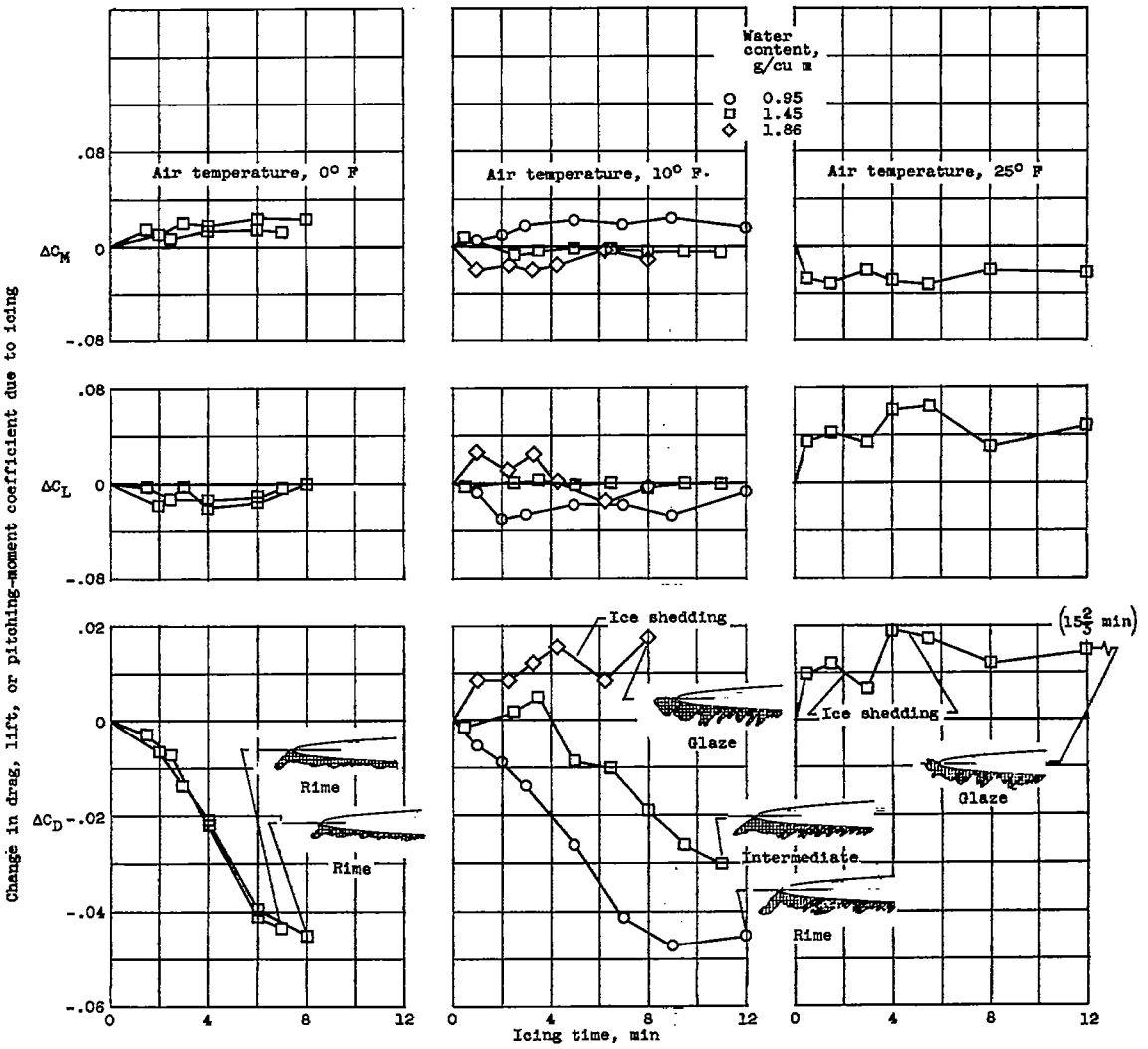

(f) Angle of attack, 8.8°; airspeed, 152 knots.

Figure 10. - Continued. Variation of aerodynamic coefficients with icing time.

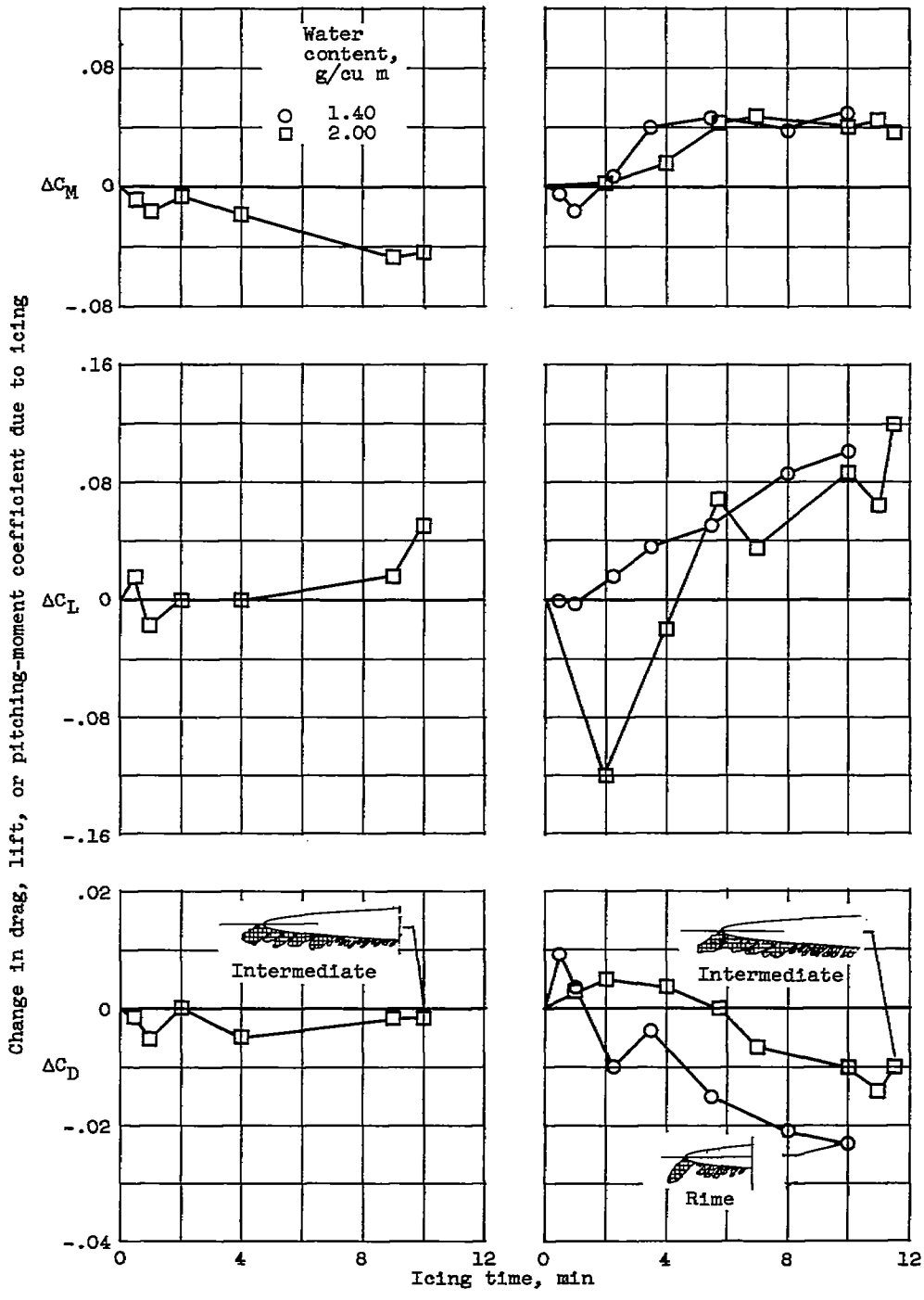

(g) Angle of attack, 10.6°; airspeed, 109 knots; air temperature, 10° F.

(h) Angle of attack, 11.6°; airspeed, 109 knots; air temperature, 10° F.

Figure 10. - Concluded. Variation of aerodynamic coefficients with icing time.

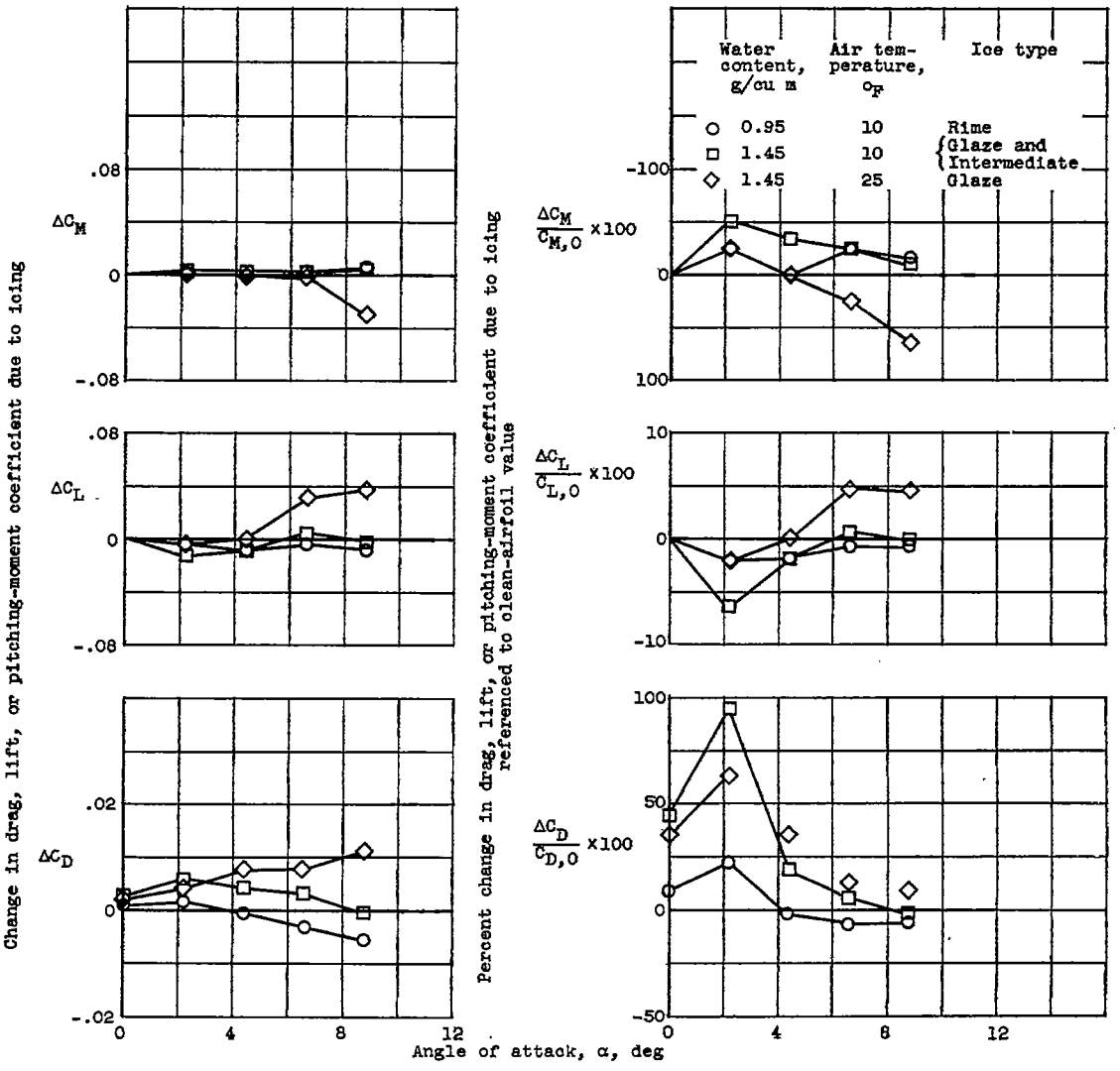

(a) Icing time, 1 minute.

Figure 11. - Variation of aerodynamic coefficients of iced airfoil as function of corrected angle of attack for two icing times. Airspeed, 152 knots.

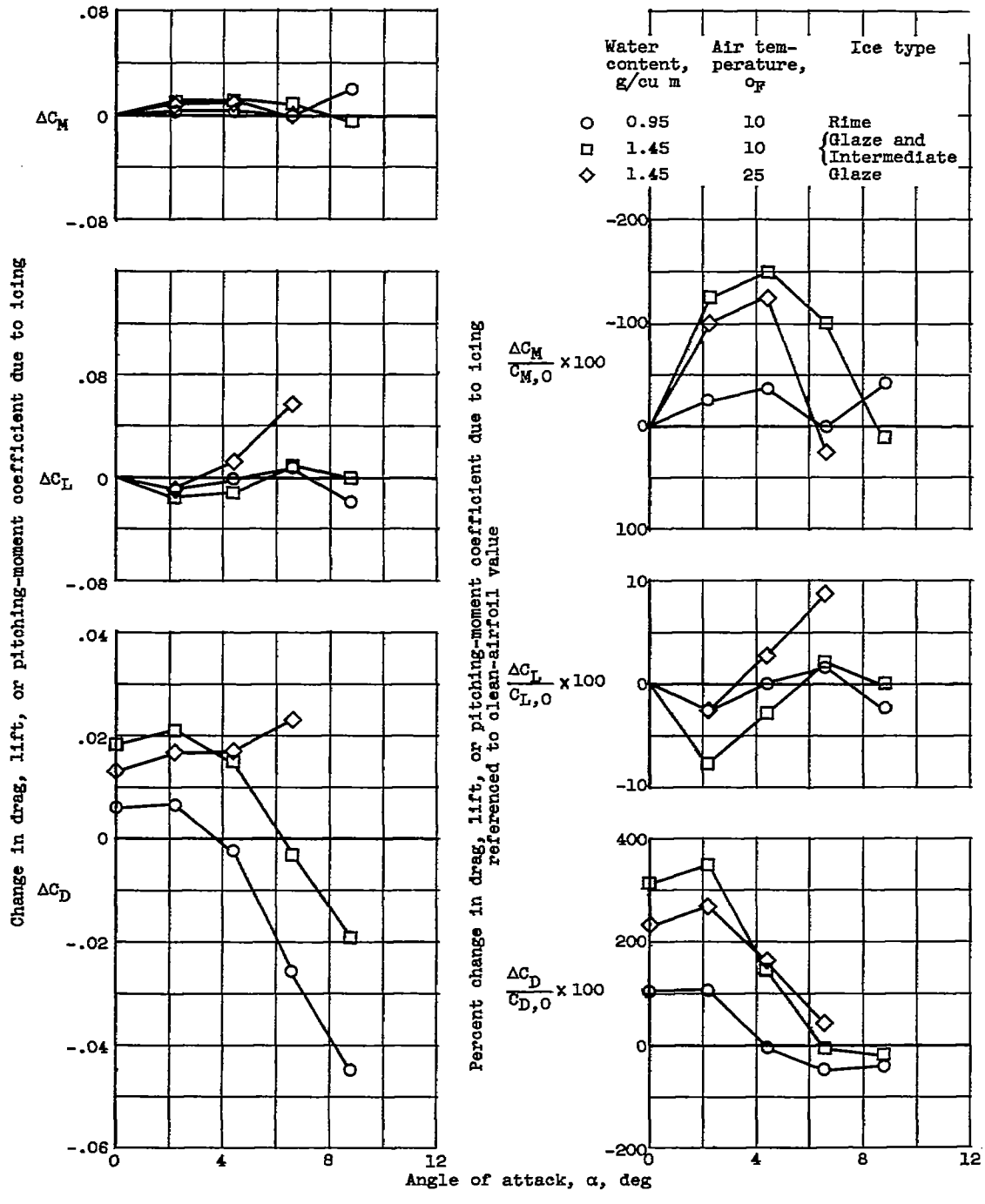

(b) Icing time, 8 minutes.

Figure 11. - Concluded. Variation of aerodynamic coefficients of iced airfoil as function of corrected angle of attack for two icing times. Airspeed, 152 knots.

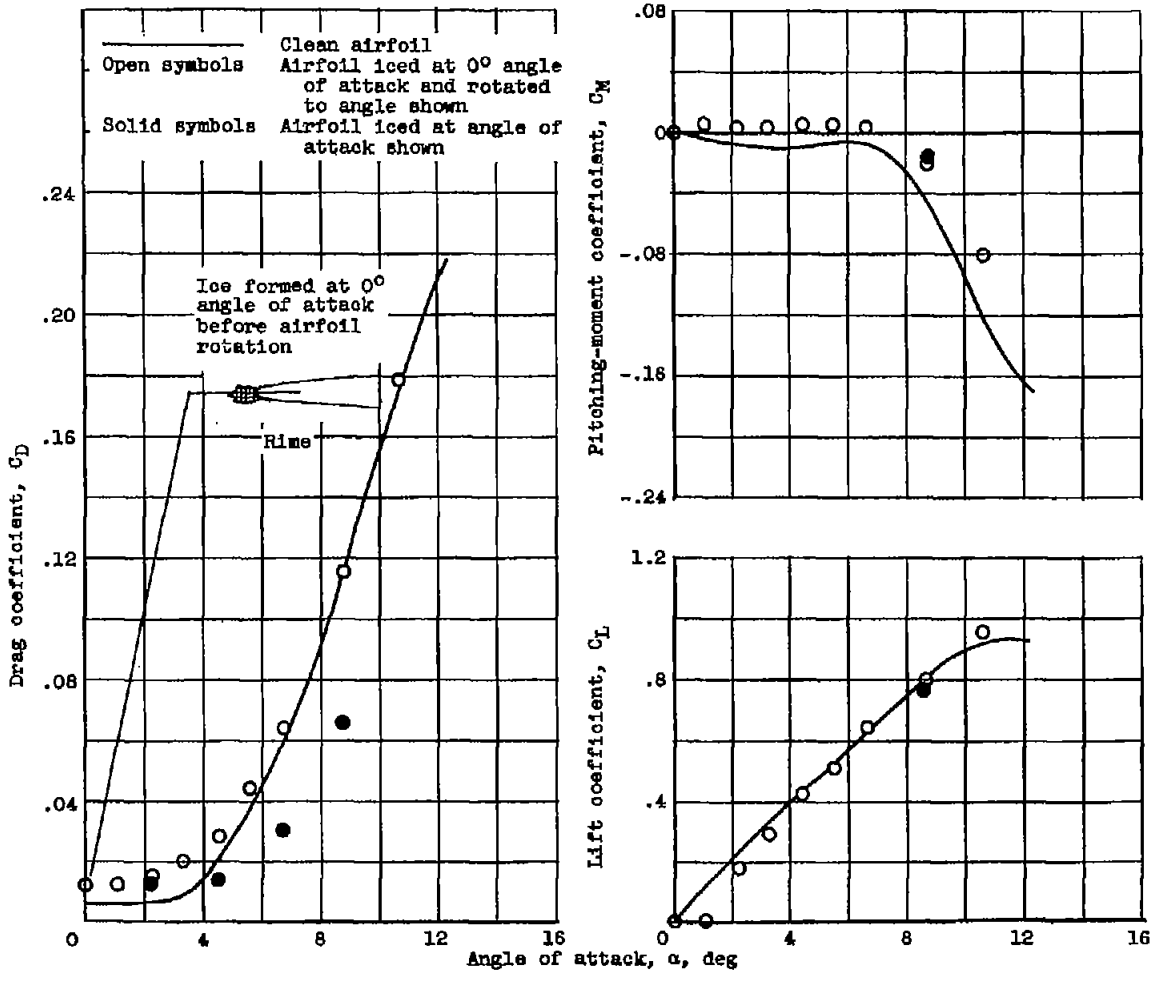

(a) Airspeed, 152 knots; air temperature, 10° F; water content, 0.95 gram per cubic meter; icing time, 10 minutes; partial ice shedding during icing time.

Figure 12. - Aerodynamic effects caused by changing angle of attack of iced airfoil.

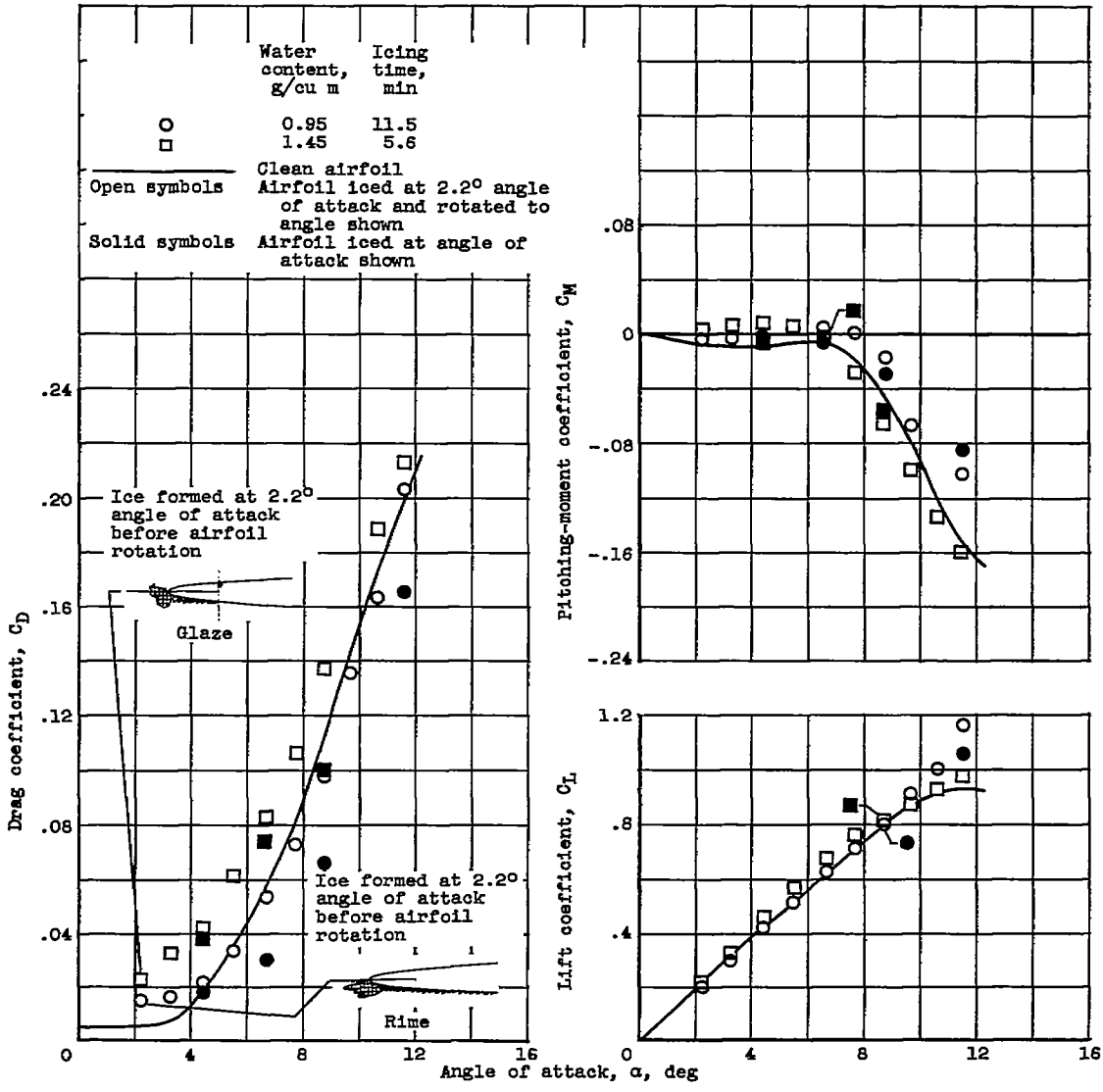

(b) Airspeed, 152 knots; air temperature, 10° F.

Figure 12. - Continued. Aerodynamic effects caused by changing angle of attack of iced airfoil.

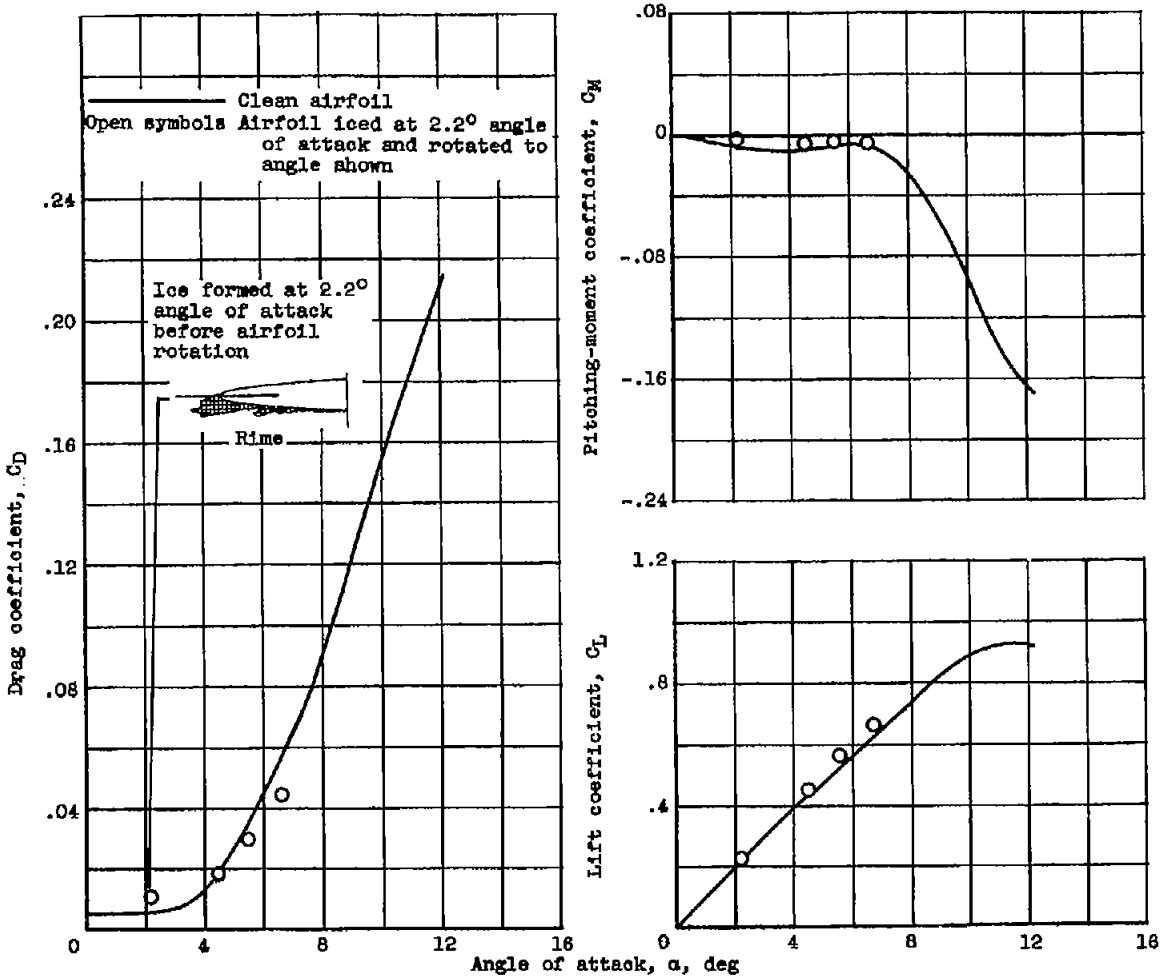

(c) Airspeed, 240 knots; air temperature, 0° F; water content, 0.90 gram per cubic meter; icing time, 10 minutes.

Figure 12. - Continued. Aerodynamic effects caused by changing angle of attack of iced airfoil.

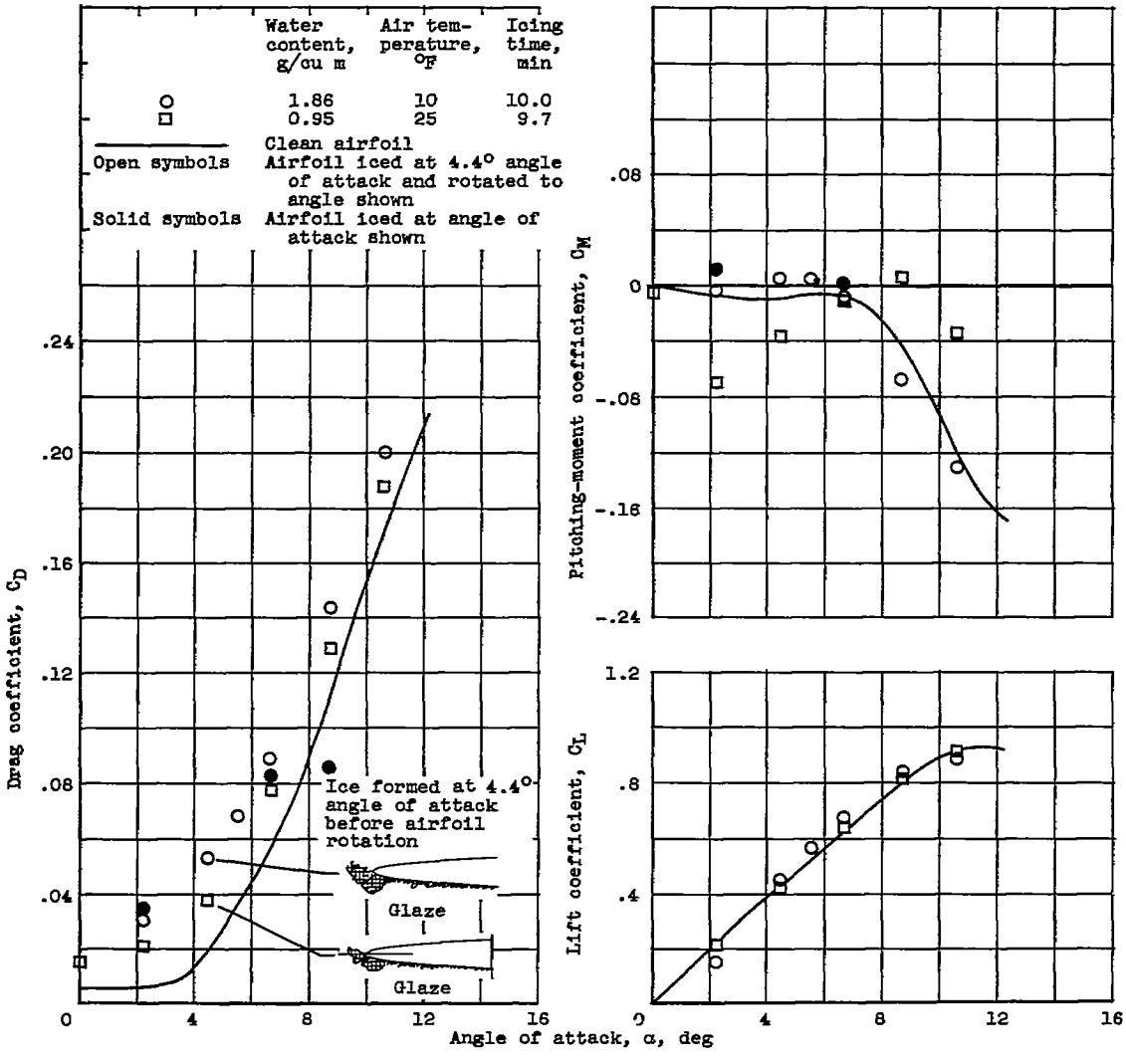

(d) Airspeed, 152 knots.

Figure 12. - Continued. Aerodynamic effects caused by changing angle of attack of iced airfoil.

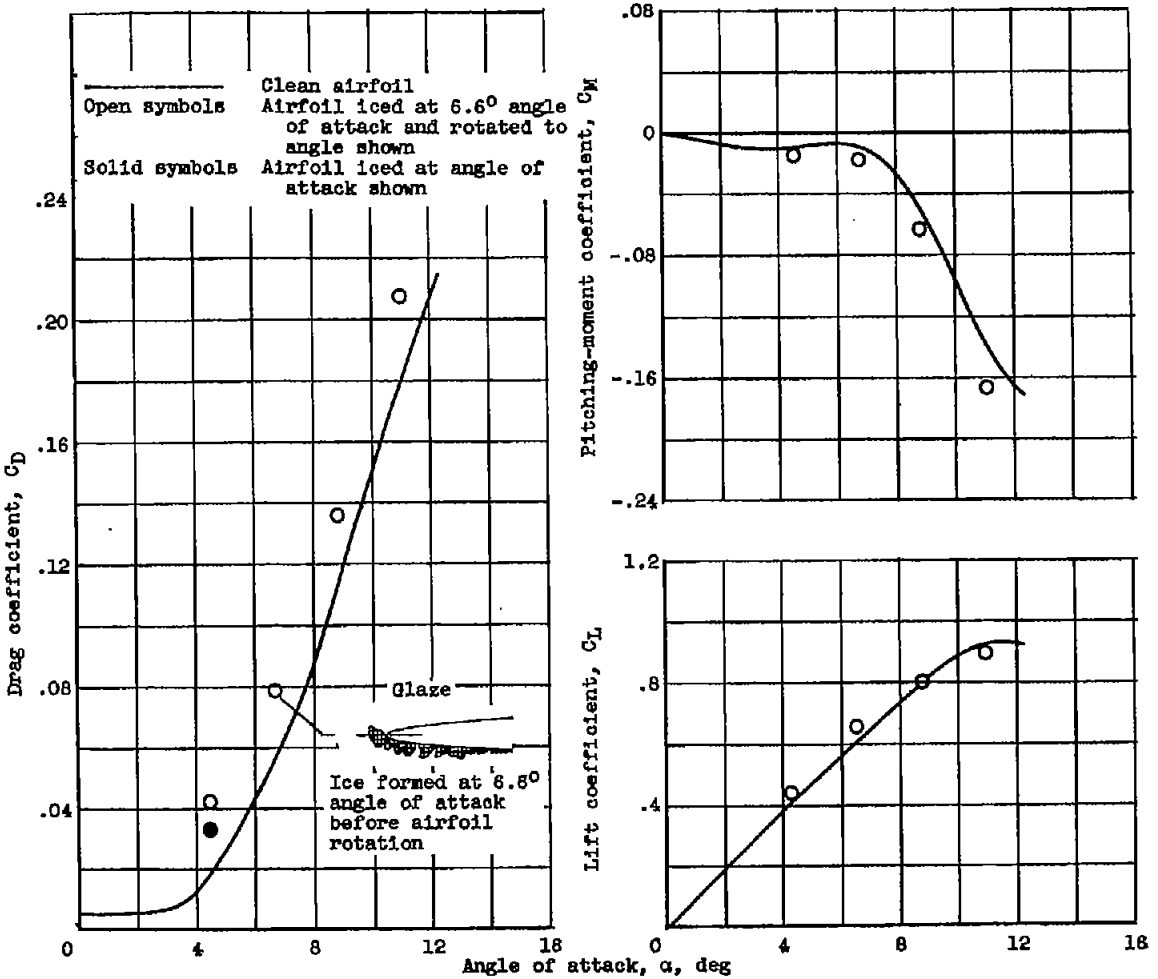

(e) Airspeed, 152 knots; air temperature, 25° F; water content, 1.45 grams per cubic meter; icing time, 10 minutes.

Figure 12. - Continued. Aerodynamic effects caused by changing angle of attack of iced airfoil.

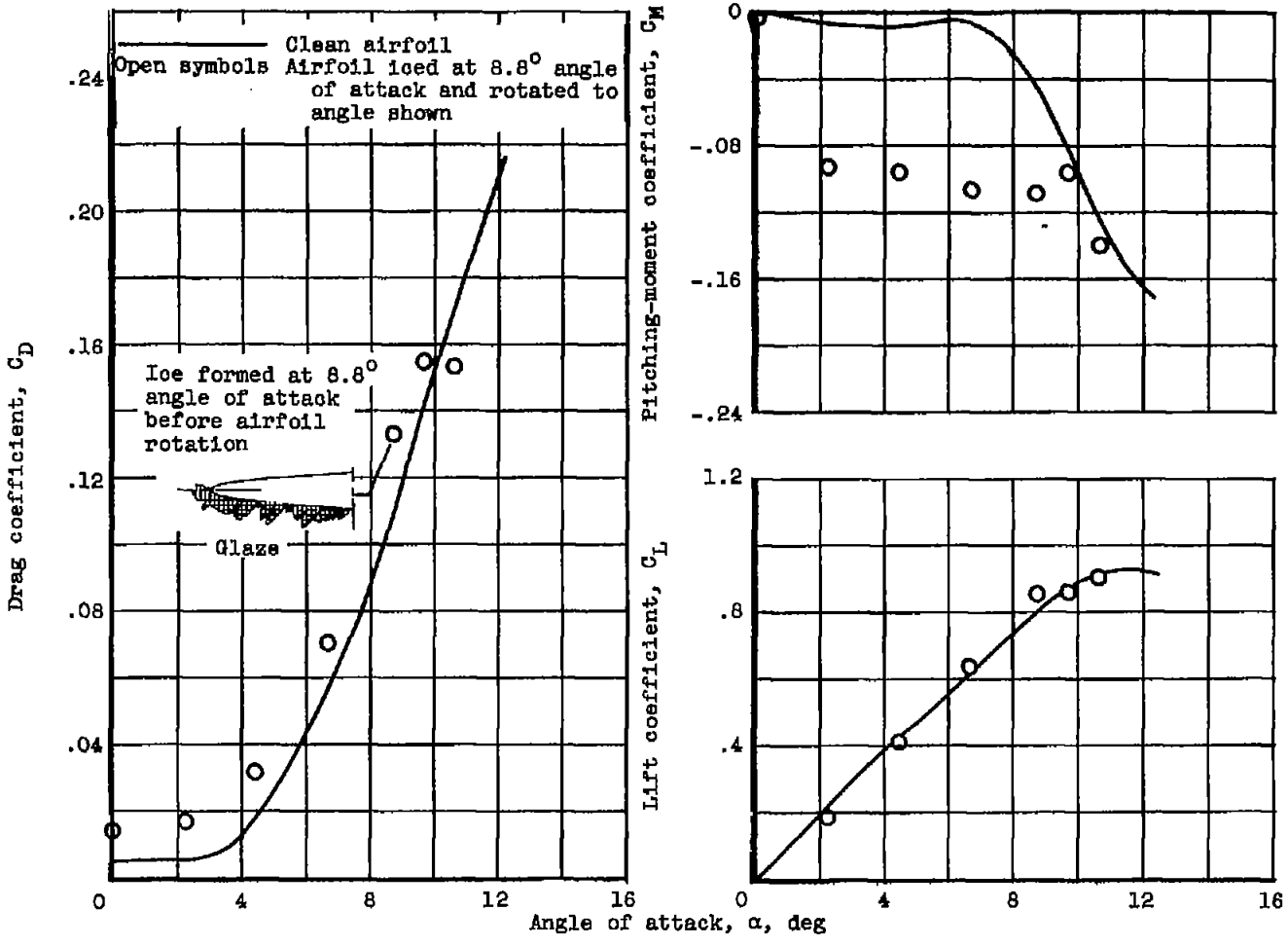

(f) Airspeed, 152 knots; air temperature, 25° F; water content, 1.45 grams per cubic meter; icing time, $15\frac{1}{4}$ minutes.

Figure 12. - Concluded. Aerodynamic effects caused by changing angle of attack of iced airfoil.